Journal of Drug Delivery Science and Technology 86 (2023) 104745

Contents lists available at ScienceDirect

Journal of Drug Delivery Science and Technology

journal homepage: www.elsevier.com/locate/jddst

Aptamer-grafted, cell membrane-coated dendrimer loaded with doxorubicin as a targeted nanosystem against epithelial cellular adhesion molecule (EpCAM) for triple negative breast cancer therapy

Afsana Sheikh [a], Mohammed A.S. Abourehab [b,c], Alaa S. Tulbah [c], Prashant Kesharwani [a,*]

[a] Department of Pharmaceutics, School of Pharmaceutical Education and Research, Jamia Hamdard, New Delhi, 110062, India
[b] Department of Pharmaceutics and Industrial Pharmacy, College of Pharmacy, Minia University, Minia, 61519, Egypt
[c] Department of Pharmaceutics, College of Pharmacy, Umm Al-Qura University, Makkah, 21955, Saudi Arabia

ARTICLE INFO

Keywords:
Triple-negative breast cancer
Dendrimer
Red blood cells
Aptamer
EpCAM

ABSTRACT

The major issue associated with chemotherapeutics is the non-specific distribution, extended range of toxicity, and low intratumoral accumulation. Targeted therapy using aptamers could be a ground-breaking approach in cancer treatment. Poly(amidoamine) PAMAM dendrimers are a type of nanocarriers with a well-defined structure, higher encapsulation efficiency and modification surface groups. However, the toxicity of cationic dendrimers and non-targetability poses a great risk to patients' health. Considering this, we developed a EpCAM aptamer-functionalized, red blood cell (RBC) membrane-camouflaged PAMAM dendrimer loaded with doxorubicin to selectively target EpCAM-positive triple-negative breast cancer (TNBC) cells. An increase in size of doxorubicin (Dox) loaded PAMAM was observed from 11.34 nm to 108.4 nm post coating with RBC membrane and aptamer, respectively. The biocompatibility and blood circulation time were enhanced by the coating of the RBC membrane on the surface of the dendrimers while functionalization with aptamers improved its cancer cell internalization. The results obtained suggested that the coating with RBC provided controlled and sustained release during the 140 h of study. *In vitro* cell viability study showed enhanced apoptosis and significantly elevated uptake by the cancer cells as compared with the non-targeted preparation. Furthermore, the volume of the tumor was significantly reduced in groups treated with aptamer-modified, cell membrane-coated dendrimer due to selective internalization in the cancer cells only. This novel, personalized, and targeted therapy could be a potent platform for TNBC therapy.

1. Introduction

Breast carcinoma is a mixed ailment rather than a mere homogenous disease. Following this path, identifying subtypes of breast cancers and specific targets to reduce their progression is a potential treatment strategy. Triple-negative breast cancer (TNBC) is one such subtype that is clinically characterized by a lack of progesterone, estrogen, and human epidermal growth factor 2 receptors contributes to its paucity of effective treatment. Reduced overall survival (10.2 months), high relapse rate, and progression-free survival (5–6 months) demonstrate the poor prognosis of TNBC. Chemotherapy is still the mainstay of treatment. Anti-microtubule agents such as taxanes, alkylating agents such as cyclophosphamide and anthracycline or DNA-intercalating agent along with 5-fluorouracil (5-FU) are often what oncologists reach for to treat TNBC [1–8].

An anthracycline class medication, doxorubicin has been explored for most cancers to date. However, its short half-life and cardiotoxicity confine its therapeutic potential. Despite aforementioned chemotherapeutics, the prognosis of TNBC is highly poor as the antitumor potential of such agents could attain plateau. Consequently, the futuristic framework holds targeted, combination, and gene therapy which could augment therapeutic response in disease subsets. Even though combination therapy and early detection can improve the rate of survival, ground-breaking methods are still required to reduce the associated side effects. Some research is now leaning towards improving the potential of existing drugs by developing novel drug delivery systems. Several

* Corresponding author. Assistant Professor & Ramanujan Fellow Department of Pharmaceutics, School of Pharmaceutical Education and Research, Jamia Hamdard, New Delhi, 110062, India.
E-mail address: prashantdops@gmail.com (P. Kesharwani).

https://doi.org/10.1016/j.jddst.2023.104745
Received 23 March 2023; Received in revised form 30 June 2023; Accepted 6 July 2023
Available online 7 July 2023

nanocarriers have been studied including micelles, liposomes, polymeric drug conjugates, lipoplexes, dendrimers, and inorganic nanoparticles for TNBC [9–20].

Dendrimers are three-dimensional macromolecular structures comprising a hydrophobic core and hydrophilic branches mimicking a tree [12,21–23]. The unique structure exemplifies dendrimers from other investigated nanocarriers and have numerous advantages. The low polydispersity affords astonishingly consistent efficacy, high loading potential, and passive targeting prospect offered by the size of dendrimer and globular structures which could deliver both hydrophobic and hydrophilic agents, advancing their therapeutic profile [24–27]. poly(amidoamine) (PAMAM) dendrimer is the first developed class of dendrimer for clinical demonstration. PAMAM has been explored in the drug delivery industry as they can hold poorly soluble drugs inside their vacant cavity while the hydrophilic moieties along with targeting ligands, antibodies, deoxyribose nucleic acid (DNA), or ribonucleic acid (RNA) could be conjugated or attached (whichever is efficient) to the peripheral functional groups. Nanometric size, scalability, and ease of fabrication are some ascendancies that made dendrimers important carriers for numerous therapeutic agents. Our group developed a 3, 4-difluorobenzylidene curcumin (CDF)-loaded hyaluronic acid-coated PAMAM dendrimer to investigate the effect on pancreatic cancer cells. As hyaluronic acid shows a strong propensity towards CD44 receptors, the targeted preparation demonstrated 1.71 times increased half maximal inhibitory concentration (IC50) value as compared with the non-targeted dendrimer [28]. The active targeting ability has also been investigated in numerous research by conjugating ligands such as arginine-glycine-aspartate (RGD) [24], folic acid (FA) [29], biotin [30], human epidermal growth factor receptor-2 (HER-2) [31], aptamers [32], and small interfering RNA (siRNA) [33]. Another study reported the delivery of doxorubicin by attaching it via a succinate linker on a third-generation glucoheptoamidated poly(amidoamine) dendrimers to glioma cells. The results showed significant apoptosis and cell cycle arrest at the G2/M phase. The conjugated system showed 4.5-fold improved anticancer response than with the drug alone, indicating a promising effect of dendrimer in mitigating glioma cells [34].

The cationic nature of dendrimers, however, highly endorses interaction with red blood cells (RBCs), questioning their safety profile. High interaction with dendrimers can rupture the RBC membrane and potentiates cytotoxicity that limits its use [35–38]. The positioning of natural cell membranes over the surface of chemical therapeutic entities facilitates man-made vectors to share similar functionalities and merits developed by the nature. Such a revolution transformed the pharmaceutical industry by biomimicking natural human physiology. PEGylation, for example, could enhance the biodistribution of nanoparticles while avoiding immunological response [39]. The swift clearance of dendrimers by the reticulum-endothelium system (RES) and lack of targeting capability would minimize their effective response while increasing serious adverse effects. Hence, structural modification of dendrimers could enhance the blood circulation time with increased accumulation at the site of action. In this regard, dendrimers could be coated with the RBC membrane to improve their flexibility, stability, and biocompatibility. Since RBC membranes express CD47 receptors, they easily undergo phagocytic inhibition of erythrocytes promoted by macrophages. Therefore, coating of RBC membrane on the surface of dendrimers could reduce the RES uptake and improve the blood circulation time. Nanoparticles could be tailored with patient's erythrocyte membrane to avoid the risk of unsolicited immunological response. Considering this, gambogic acid-loaded RBC membrane-coated poly (lactic-co-glycolic acid) (PLGA) nanoparticles were fabricated that accelerated the therapeutic anticancer response in SW480 implanted Balb/c mice [40]. RBC-camouflaged cells could improve the blood circulation time, but the major problem associated is non-targeting potential.

Aptamers are single-stranded oligonucleotide with high binding capacity and selectivity towards targeted cells. Aptamers offer profound benefits over monoclonal antibodies due to high robustness, low immunogenicity, and increased penetration [41]. An aptamer-functionalized drug delivery system could be a revolutionizing approach in cancer treatment, especially for TNBC. The versatility of aptamers enables them to fit into the pockets of targets prompting magnificent binding efficacy.

Epithelial cell adhesion molecule (EpCAM) is a cancer-associated antigen overexpressed on TNBC cells, making it an important target for this malignancy. EpCAM is one of the earliest identified targets in TNBC. Nonetheless, not much clinical progress has been made to target and mitigate this antigen [42]. In a study, nearly 2 of 3 TNBC cells showed strong expression for the EpCAM oncogenic protein, which is linked to poor prognosis [43]. It has been demonstrated that an EpCAM-functionalized single-walled carbon nanotube (SWCNT) induced higher apoptosis than non-targeted therapy in EpCAM-positive cells for the treatment of breast carcinoma [44].

The development of a highly advanced targeted therapy should emphasize sufficient drug loading, enhanced permeation, elevated biocompatibility, increased circulation, high tumor internalization, and accumulation. Further, the targeted preparation should contain nano-oncotherapeutics. Our targeted therapy was customized to accomplish the primary demand for cancer therapy.

Herein, we developed a targeted RBC membrane-camouflaged drug-loaded PAMAM dendrimers for TNBC therapy. In this study, doxorubicin (Dox) was entrapped within the core of PAMAM dendrimers and then layered with the RBC membrane, making it a biomimetic therapeutic system. Next, the camouflaged drug-loaded nanoparticle was tagged with EpCAM aptamers to selectively deliver to the cells of TNBC only. The efficacy and safety profile were estimated *in vitro* and *in vivo*.

2. Materials and methods

2.1. Materials

4.0G PAMAM dendrimers, 3-[4,5-dimethylthiazol-2-yl]-2,5 diphenyltetrazolium bromide MTT and doxorubicin (Dox) were obtained from Sigma Aldrich. EpCAM aptamer (5′-amino-CAC TAC AGA GGT TGC GTC TGT CCC ACG TTG TCA TGG GGG GTT GGC CTG-3) was obtained from Santa Cruz Biotechnology. N-hydroxy succinimide (NHS) and N-(3-dimethyl aminopropyl)-N-ethylcarbodiimide (EDC) were obtained from Loba Chemie. All other chemicals were of reagent grade and were used without any modifications.

2.2. Development of Dox-loaded PAMAM dendrimers (Dox-PAMAM)

Dox (2 mg) was dissolved in 4 ml of Dimethyl sulfoxide (DMSO) and allowed to stir overnight in a dark room. Next, the drug solution was added to a vial containing 20 mg of 4.0G

poly(amidoamine) (PAMAM) and the reaction were carried out for 24 h. Afterward, phosphate-buffered saline (PBS) was added and extracted with a sufficient quantity of ethyl acetate to remove the free drug. The solution was lyophilized further to obtain dark red preparation of Dox-loaded PAMAM. The encapsulation efficiency (EE%) and drug-loading capacity (DL%) of Dox were determined by spectrophotometric technique at 480 nm [45].

2.3. Development of RBC membrane-derived vesicles

The RBC membrane was extracted according to a previously published protocol [46]. Briefly, 5 ml of blood was isolated from Balb/c mice (19–23g) and collected in a heparin-filled vacutainer. To separate the RBCs, PBS (3 ml) was added to the blood and the mixture was centrifuged at 3000 rpm for 5 min at 4 °C. After removing the serum, the suspension was irrigated with ice-cold PBS several times to remove the buffy coat. Nearly 0.25 × PBS was then added to the prepared RBC and again centrifuged at 10,000 rpm at 4 °C to eliminate hemoglobin and

acquire pink-colored ghost pellets of RBC. The RBC ghost was then sonicated in a capped vial for 5 min. The RBC membrane was then stored at −80 °C post-lyophilization.

2.4. Grafting of Dox-loaded PAMAM dendrimers with RBC membrane (RBC-Dox-PAMAM)

RBC membrane (2 mg) was stirred with Dox-PAMAM (4 mg) in a vial containing PBS for 2 h. The solution was then sonicated using a bath sonicator for 10–15 min. The RBC membrane was enveloped over PAMAM through electrostatic interaction. The success of coating was ascertained by measuring the size and zeta potential of obtained camouflaged nanoparticulate system [47].

2.5. EpCAM aptamer conjugation of RBC-Dox-PAMAM

The carboxylic acid of EpCAM aptamer was activated using EDC and NHS. 10 μl of EDC/NHS solution (2 mg in 200 μL DNase RNase free water) was stirred with 600 μg aptamer in 500 μL water and stirred at 4 °C for 3 h. The resultant solution was filtered to remove excess EDC and NHS. The activated EpCAM aptamer was then added to the solution of RBC-Dox-PAMAM (2 mg/ml) and stirred for 24 h at 4 °C. The resultant mixture was centrifuged at 10,000 rpm for 15 min to remove the unconjugated aptamer [48,49].

2.6. Characterization of Dox-PAMAM, RBC-Dox-PAMAM, and Apt-RBC-Dox-PAMAM

The physical state of doxorubicin and Dox-PAMAM was examined using differential scanning calorimetry (DSC) with approximately 5 mg of samples heated at a temperature within the range of 40°C–400° with a heating rate of 10 °C/min in an aluminum pan under a constant nitrogen flow rate. The Fourier transform infrared spectra of pure drug and Dox-PAMAM were recorded and obtained using Bruker FTIR spectrometer in the region of 400 to 4000 cm^{-1} [50]. ^1H NMR spectra of G4 PAMAM dendrimers and Dox-PAMAM were obtained using D_2O water as the solvent at room temperature with 400 MHz. MestReNova software was then used to locate and interpret the obtained peaks. The particle size and zeta potential were investigated using dynamic light scattering (DLS) technique [51]. Encapsulation success of doxorubicin was also estimated by the fluorescence spectrometric method using 560 nm at λem and 480 nm at λex. The morphology of the obtained nano-therapeutic system was examined by transmission electron microscope (TEM) and atomic force microscope (AFM).

2.7. Doxorubicin release profile from the complex

The release profile of doxorubicin was recorded at the pH of blood (i.e., pH 7.4) and the pH of lysosomes (i.e., pH 5.5) using equilibrium dialysis method. The fabricated preparations equivalent to the weight of 10 mg was sealed in a dialysis bag, having a molecular weight cut off of nearly 10 kDa. The bag was then immersed in beakers containing 50 ml of buffer (pH 7.4 and 5.5) and was incubated in an incubator shaker. 1 ml of outer phase medium was withdrawn at specific time intervals while simultaneously replacing it with an equivalent amount of buffer with the same pH as the dialysis medium. The amount of drug release was determined by the spectrometric technique at a predefined time [52,53].

2.8. Cell viability assay

To understand the cellular effect of the free drug (Dox), RBC-Dox-PAMAM and Apt-RBC-Dox-PAMAM having an equivalent Dox dose of 0.5 μg/ml, 1.5 μg/ml, 2.5 μg/ml, 5 μg/ml and 10 μg/ml, MTT assay was executed on 4T1 (EpCAM-positive cell line) and MDA-MB-231 (EpCAM-negative cell line) cells. Primarily, the cells (5000 cells/well) were cultured in a 96-well plate and incubated at 37 °C in 5% CO_2. The cells were then treated with the free drug, RBC-Dox-PAMAM or Apt-RBC-Dox-PAMAM for 6 h. After refreshing the media, the cells were again incubated for 48 h maintaining 37 °C atmospheric conditions. 5 mg/ml of MTT solution in PBS (20 μL) was then added to each well and incubated further for 4 h. After aspiration of media, DMSO (100 μL) was added further to dissolve the developed formazan crystals. At last, the SpectraMax Ò M2 microplate reader was employed to record the optical absorbance at 570 nm, while the 630 nm range was used for reference [54].

2.9. Cellular uptake

The uptake ability of targeted and non-targeted RBC-camouflaged doxorubicin-loaded dendrimers was studied. 4T1 cells were seeded at a density of 5×10^4 cells/well and nurtured keeping them undisturbed for 24 h. The cells were further treated with plain RBC-Dox-PAMAM and Apt-RBC-Dox-PAMAM for 2 h at 37 °C in a serum-free media. Next, the cells were further washed three times with PBS to confiscate extracellular deposits and fixed with 4% paraformaldehyde at 20 °C for 20 min. The coverslips were then fixed on the slides and scanned using confocal microscope.

2.10. In vivo therapeutic efficacy study

The *in vivo* antitumor study was carried out in female Balb/c mice after approval from the institutional animal ethics committee (IAEC) of Jamia Hamdard (Protocol no. 1734). 4T1 cells (5×10^5) in PBS (0.1 ml) at pH 7.4 was administered subcutaneously to the right flank of female Balb/c mice weighing 19–23g for the development of 4T1 tumor-bearing mice. When the size of the tumors reached 30 mm^3, the animals were randomly divided into a group of 4 (n = 6) and treated with 200 μL of plain Dox, RBC-Dox-PAMAM or Apt-RBC-Dox-PAMAM (equivalent to 5 mg/kg of Dox). All preparations were administered via the tail vein while those that received PBS were kept as negative control. The tumor volume was recorded using the below formula:

$$\text{Tumor volume } (mm^3) = \text{length} \times \text{width} \times \text{height}/ \quad 2$$

The weight of the mice along with tumor weight were also recorded to estimate the therapeutic efficacy and desired toxicity of the targeted preparation in comparison to plain drug and non-targeted therapy [55].

2.11. Pathological evaluation of systemic toxicity

Thirty days post-treatment with Apt-RBC-Dox-PAMAM, RBC-Dox-PAMAM, plain Dox or PBS, the mice were euthanized and the systemic toxicity on major vital organs was observed. On such note, heart, liver, kidney, spleen, and tumors were isolated, irrigated with PBS, and fixed with 10% formalin solution. The tissues were entrenched afterward in paraffin and stained with hematoxylin and eosin (H&E) to obtain images under 40x using an inverted optical microscope [55].

2.12. Statistical analysis

The results of the quantitative analysis of the study data, which were collected in triplicate, were expressed as mean and standard deviation (SD). One-way analysis of variance (ANOVA) was used in the statistical analysis, which was carried out using the GraphPad prism. A p-value of 0.05 or less was regarded as statistically significant.

3. Result and discussion

3.1. Development and characterization of Dox-PAMAM

The PAMAM dendrimer is a highly organized globular-shaped

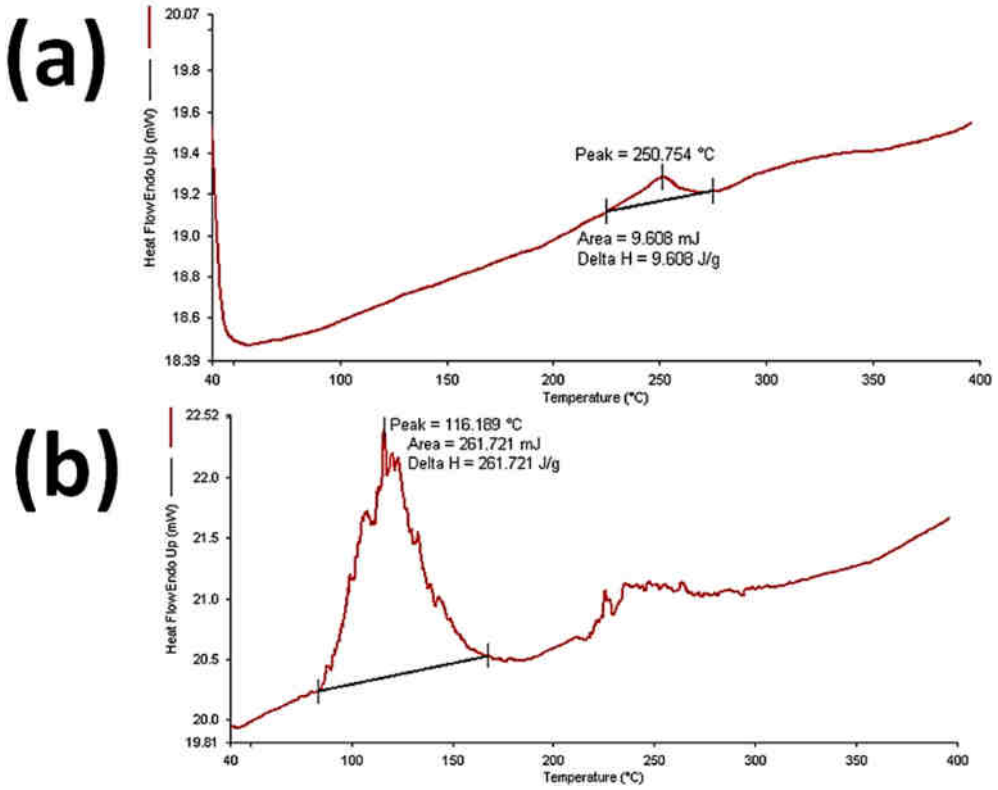

Fig. 1. Differential scanning calorimetric analysis of Dox (a) and Dox-PAMAM (b).

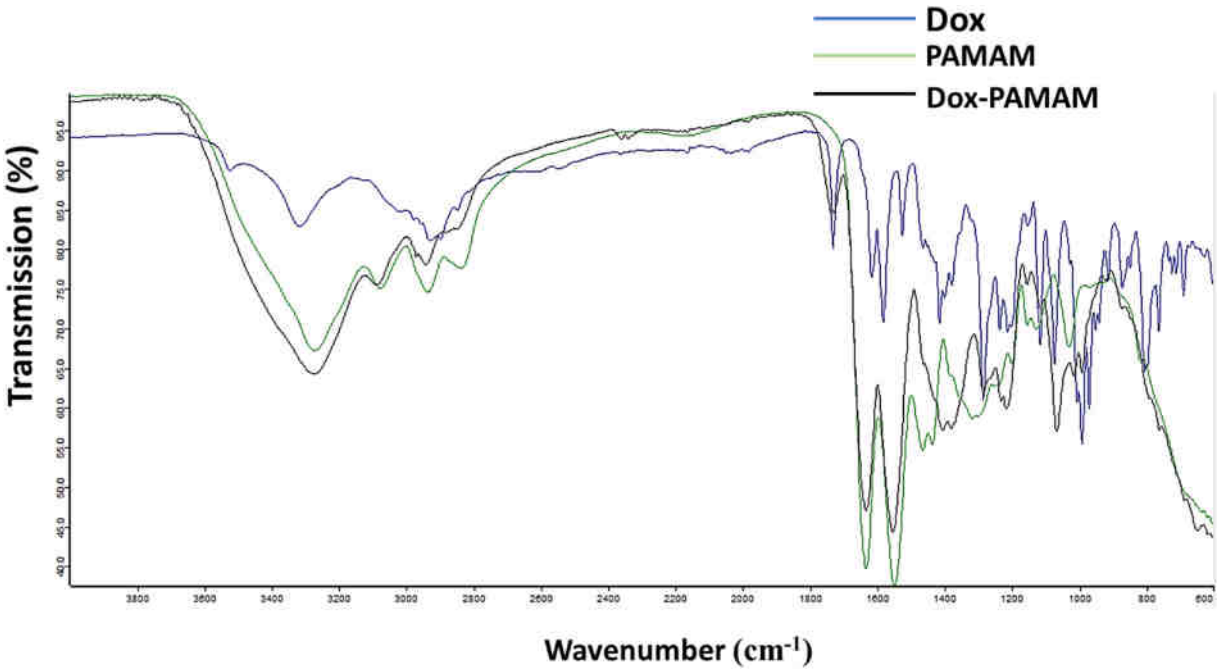

Fig. 2. Fourier transform spectroscopic study of Dox, PAMAM and Dox-PAMAM.

structure known for its potential to encapsulate hydrophobic compounds inside the core. Doxorubicin is a hydrophobic compound with subtherapeutic efficacy despite DNA-intercalating properties. Moreover, low absorption and high rate of elimination limits its clinical use. Hence, we employed PAMAM dendrimers to entrap doxorubicin to expand its therapeutic window. The encapsulated entities demonstrate the presence, absence, or relocation of peaks owing to the alteration in a crystalline lattice, boiling sublimation, or melting point providing information related to the quantitative and qualitative information of molecular entities residing inside the complex structures. The DSC thermogram of pure doxorubicin showed an endothermic peak at 250.75 °C. The elimination of such peak in doxorubicin-loaded PAMAM dendrimers confirms excellent drug encapsulation (Fig. 1 a and b) [56]. The absorption peaks of pure-drug doxorubicin and Dox-PAMAM

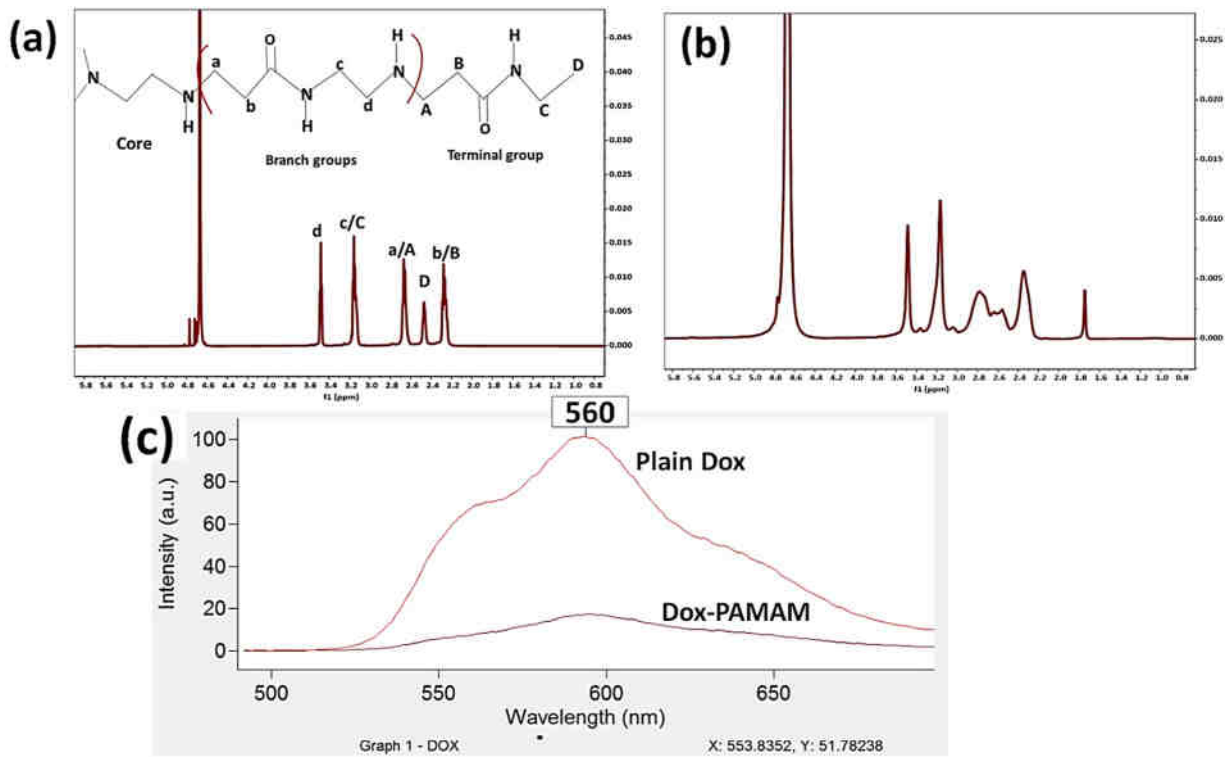

Fig. 3. Nuclear magnetic resonance-based analysis of PAMAM (a) and Dox-PAMAM (b); fluorescence spectroscopic study of Dox and Dox-PAMAM.

obtained by fourier-transform infrared (FTIR) spectrometer are shown in Fig. 2. Doxorubicin showed characteristic peaks at 3525 and 3316 cm^{-1}, which are accredited to O–H and N–H stretching vibrational groups. The C═O group showed stretching vibration at 1727 cm^{-1}, confirming the purity of drug. The G4 PAMAM dendrimers showed characteristic absorption bands at 3301 cm^{-1}, 3077 $cm^{-1,}$ and 1248 cm^{-1} which are attributed to N–H stretching vibrations of amines, antisymmetric vibration of primary substituted amine and C–H stretching, while peaks at 1547 cm^{-1}, 1463 cm^{-1}, 1316 cm^{-1} is due to N–H bending of substituted amine. The peak at 1125 cm^{-1} is due to C–C bending of PAMAM dendrimers. In Dox-PAMAM spectra, an upshift of C═O stretch of doxorubicin is observed, which indicates the conformational change in the appearance of drug. The major characteristic peaks are of G4 PAMAM dendrimers evidenced by the incorporation of the drug inside the core of dendrimer. Thus, the spectra obtained by FTIR have been offset for simplicity [57–59]. The ^{1}H NMR spectra of the dendrimers and the formulation are represented in Fig. 3. The intensified peak at 3.5 ppm corresponds to the methylene protons 'd'. The triplet peaks at a and c are assigned at 2.8 ppm and 3.4 ppm, respectively, which is due to the presence of CH_2 protons. The doublet peak at 2.6 ppm is assigned to b, which is due to CH_2/N–H protons. In the formulation, only peaks c and c are observed (Fig. 3a and b) [60]. According to the literature, doxorubicin shows a peak at 7.54 ppm and 7.70 ppm [61], which were not observed in the spectra of Dox-PAMAM (data not shown), suggesting the successful encapsulation of the drug. To confirm the encapsulation of doxorubicin in PAMAM dendrimers, a fluoroscent spectroscopic study was performed. Plain Dox showed a peak at 560 nm while no such peak was present at such wavelength indicating the successful encapsulation of drug inside the core. Our results are consistent with the other published studies (Fig. 3c) [33].

TEM and AFM images of RBC-Dox-PAMAM and Apt-RBC-Dox-PAMAM are shown in Fig. 4 suggesting that the grafted aptamer on RBC-camouflaged nanoparticle are of spherical shape. Our results are consistent with the previously published studies [62,63].

3.1.1. Drug loading and encapsulation efficiency

The drug loading and encapsulation efficiency was investigated through spectromic analysis. The loading percentage of Dox was obtained to be 37 ± 71% while the encapsulation efficiency was 57.12 ± 4.4%. Our result is in accordance with the previously published results [28].

3.2. Development of RBC membrane-camouflaged Dox-PAMAM

The RBC membrane was isolated from freshly collected blood to envelop the Dox-PAMAM and develop a nano-oncotherapeutic platform with extended biocompatibility. Since RBC membranes express CD47 glycoprotein, they are easily uptaken by phagocytosis. Thus, coating the membrane by electrostatic interaction on PAMAM dendrimers could improve the pharmacokinetic profile. DLS results revealed the size of Dox-PAMAM to be 11.34 nm which increased up to 75 nm. A futher increase in size was reported after conjugation with the aptamer (108.4 nm). Moreover, after coating with the RBC membrane, the zeta potential changed from 17.17 mV to 1.081 mV confirming the successful coating of the membrane. A further decrease in zeta potential of up to −26.53 mV was seen, indicating the conjugation of aptamer on surface of RBC-camouflaged PAMAM dendrimer (Fig. 5).

3.3. Doxorubicin release profile from the complex

The *in vitro* release profile of Dox from Dox-PAMAM and RBC-Dox-PAMAM was evaluated at different time intervals and at different pH. Since the pH of cancer cells is slightly acidic, it becomes necessary to accurately inspect the behavior or pattern of drug release at varying pH levels, especially while dealing with the targeted preparations. Aliboladi et al. found no significant difference in the release profile of gemcitabine from nanoparticles, and aptamer decorated nanoparticles, as aptamers alone, do not affect the rate of drug release but rather promotes cell uptake and internalization, providing supreme therapeutic results [64]. As illustrated in Fig. 6, the RBC-coated preparation showed a maximum of 11.58% Dox release at pH 7.4 during 60 h of

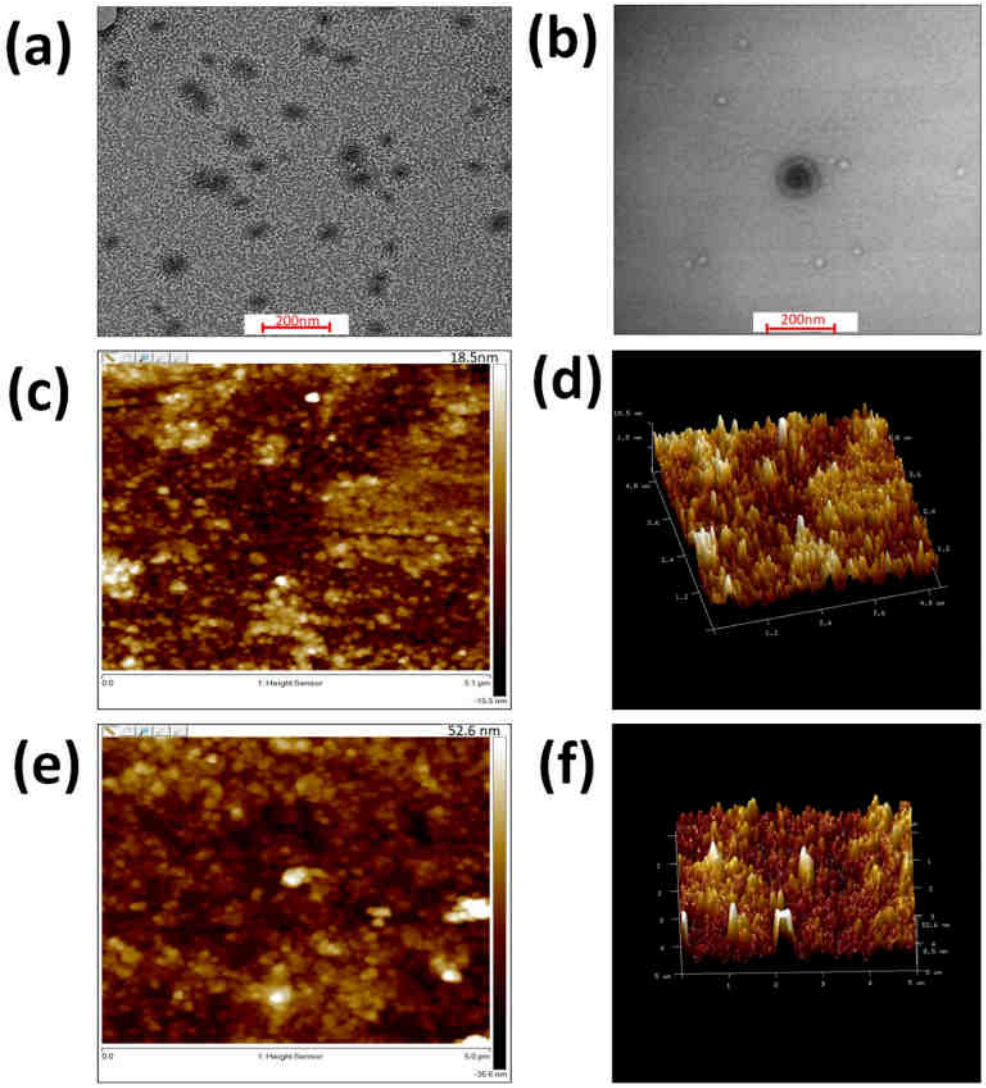

Fig. 4. Transmission electron microscopic images of Dox-PAMAM (a) and RBC-Dox-PAMAM (b); atomic force microscopic images of Dox-PAMAM (2D and 3D) (c and d) and RBC-Dox-PAMAM 2D and 3D) (e and f).

study while 58.27% and 49.23% release of Dox was detected from RBC-Dox-PAMAM and Dox-PAMAM, respectively, at pH 5.5 during the 60 h of study. A sustained release profile of Dox at physiological conditions is ascribed to the entrapment of Dox in the core of the PAMAM dendrimer. Under acidic conditions, the RBC-camouflaged system demonstrated an accelerated release pattern due to repulsive forces between the protonated $–NH_2$ group of RBC proteins and the surface of the PAMAM dendrimer, causing the detachment of the RBC membrane in presence of hydrogen ions. The inner terminal amino groups of PAMAM, protonates at acidic pH causing charge repulsion. The dendrimer adopts an "extended conformation" as a result. It is important to mention that RBCs acted as a gatekeeper for controlling the release rate, as a lower release rate of the drug was observed as compared with the uncoated Dox-P platform. This system would therefore be efficient *in vivo* due to greater release at the desired site [65].

3.4. Cell viability assay

MTT analysis illustrated the viability of cells upon treatment with plain Dox, RBC-Dox-PAMAM or Apt-RBC-Dox-PAMAM on ($EpCAM^+$) and MDA-MB-231 ($EpCAM^-$) cells. According to the data represented in Fig. 7a and b, plain doxorubicin exhibited higher toxicity than targeted and non-targeted preparations. Nevertheless, a higher cytotoxic effect was significantly discerned by Apt-RBC-Dox-PAMAM in comparison with RBC-Dox-PAMAM in the EpCAM-positive cell line ($p < 0.05$). Such an augmented effect by the EpCAM aptamer-functionalized biomimetic preparation is due to their selectivity towards specific receptors, causing receptor-mediated endocytosis. The higher binding ability of the aptamer towards EpCAM receptors illustrated efficacious results that spared the healthy cells from the deleterious impact of the cytotoxic substance. In MDA-MB-231 cells, the targeted nano-preparation failed to demonstrate a profound cell-killing effect which is due to non-selectivity towards such cells (Fig. 7b). When comparing targeted and non-targeted RBC-coated PAMAM, doxorubicin showed higher cytotoxicity, which could be due to greater and faster cellular transportation via diffusion rather than following the receptor-mediated cellular internalization.

3.5. Cellular uptake study

The preeminent feature of targeted therapy is high specificity towards the receptors overexpressed on cancer cells. Herein we evaluated the cellular internalization potential of targeted and non-targeted therapy in 4T1 cells. Hoechst 33342 was used to stain the nuclei while Dox internalization was seen by the fluorescent property of Dox. The result in Fig. 8 shows a higher internalization of doxorubicin after 2 h, while minimal fluorescence was exhibited by the untargeted preparation. An

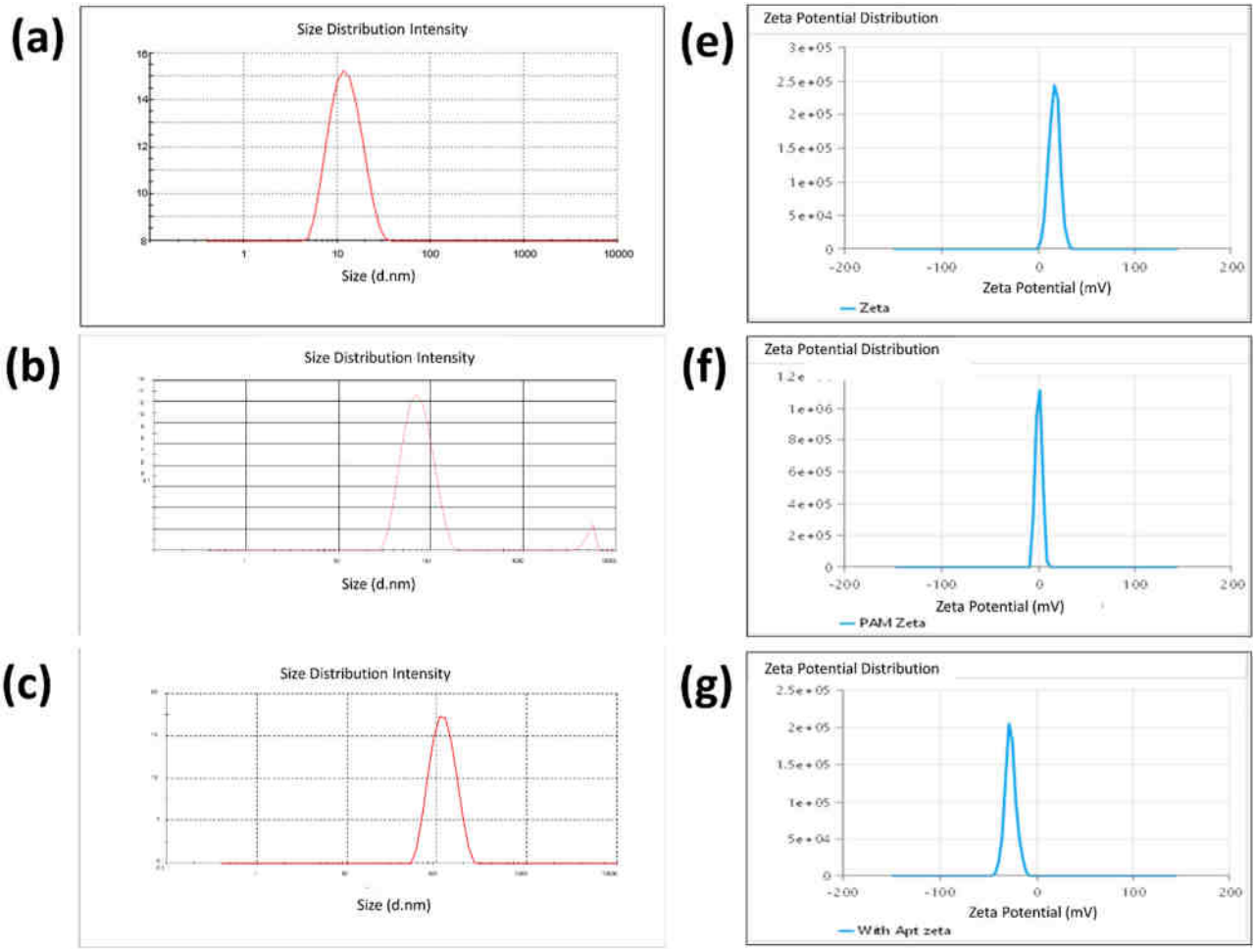

Fig. 5. Representation of particle size and zeta potential of Dox-PAMAM (a, e), RBC-coated Dox-PAMAM (b, f) and aptamer-functionalized RBC-coated Dox-PAMAM (c, g).

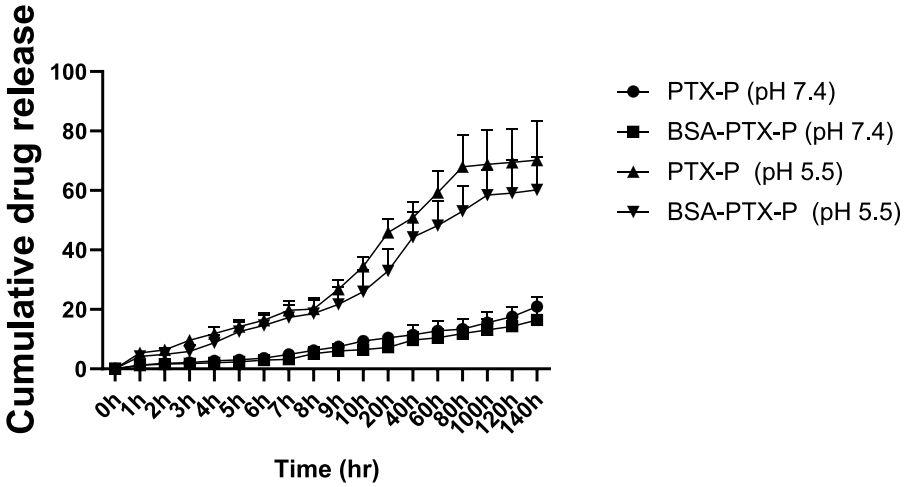

Fig. 6. Drug release profile of Dox-PAMAM and RBC-Dox-PAMAM at pH 7.4 and 5.5.

enhanced red fluorescence in the merged section shows a higher accumulation of aptamer-functionalized therapy which is due to receptor-based endocytosis. Similar results were obtained previously exemplifying the role of aptamers in targeted therapy [49,66].

3.6. *In vivo therapeutic efficacy study*

A comprehensive analysis of the therapeutic potential in terms of tumor volume, body weight loss of the drug, aptamer-mediated targeted therapy, and non-targeted therapy was performed on 4T1-laden Balb/c

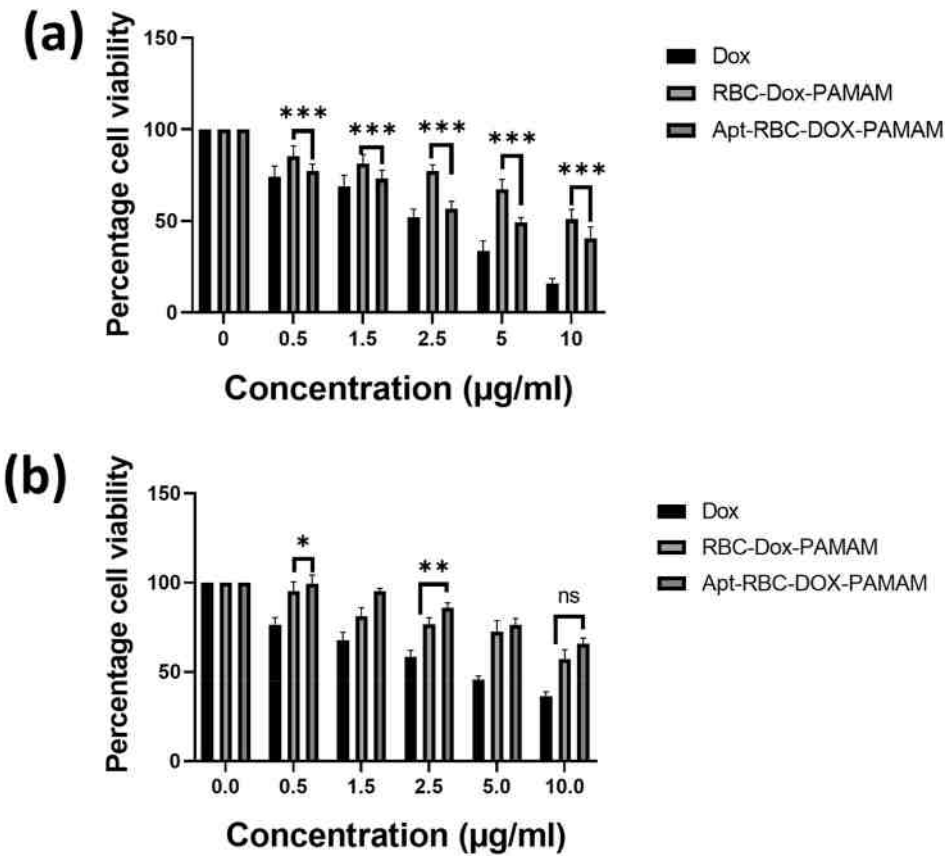

Fig. 7. Cell viability study of Dox, RBC-Dox-PAMAM and Apt-RBC-Dox-PAMAM using EpCAM-positive 4T1 cell line (a) and EpCAM-negative MDA-MB-231 cell line for 48 h (b) [**, *** and ns represents $p < 0.05$, $p < 0.001$ and non-significant, respectively].

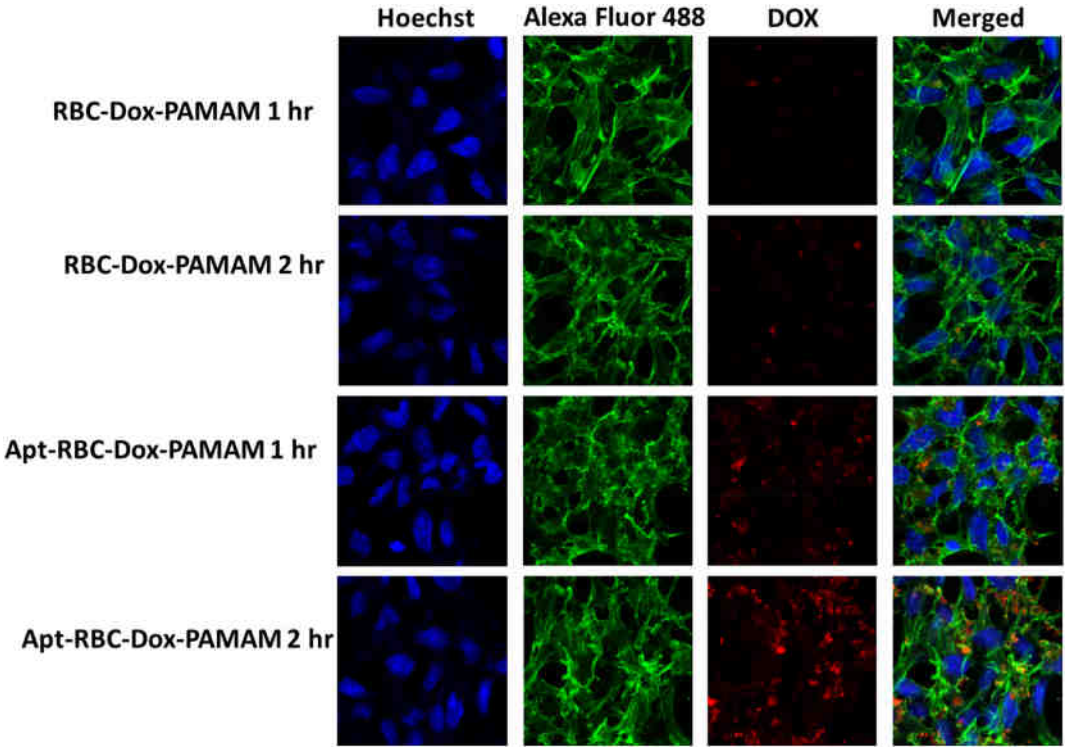

Fig. 8. Cell uptake study of RBC-Dox-PAMAM (non-targeted) and Apt-RBC-Dox-PAMAM (targeted) using a confocal microscope.

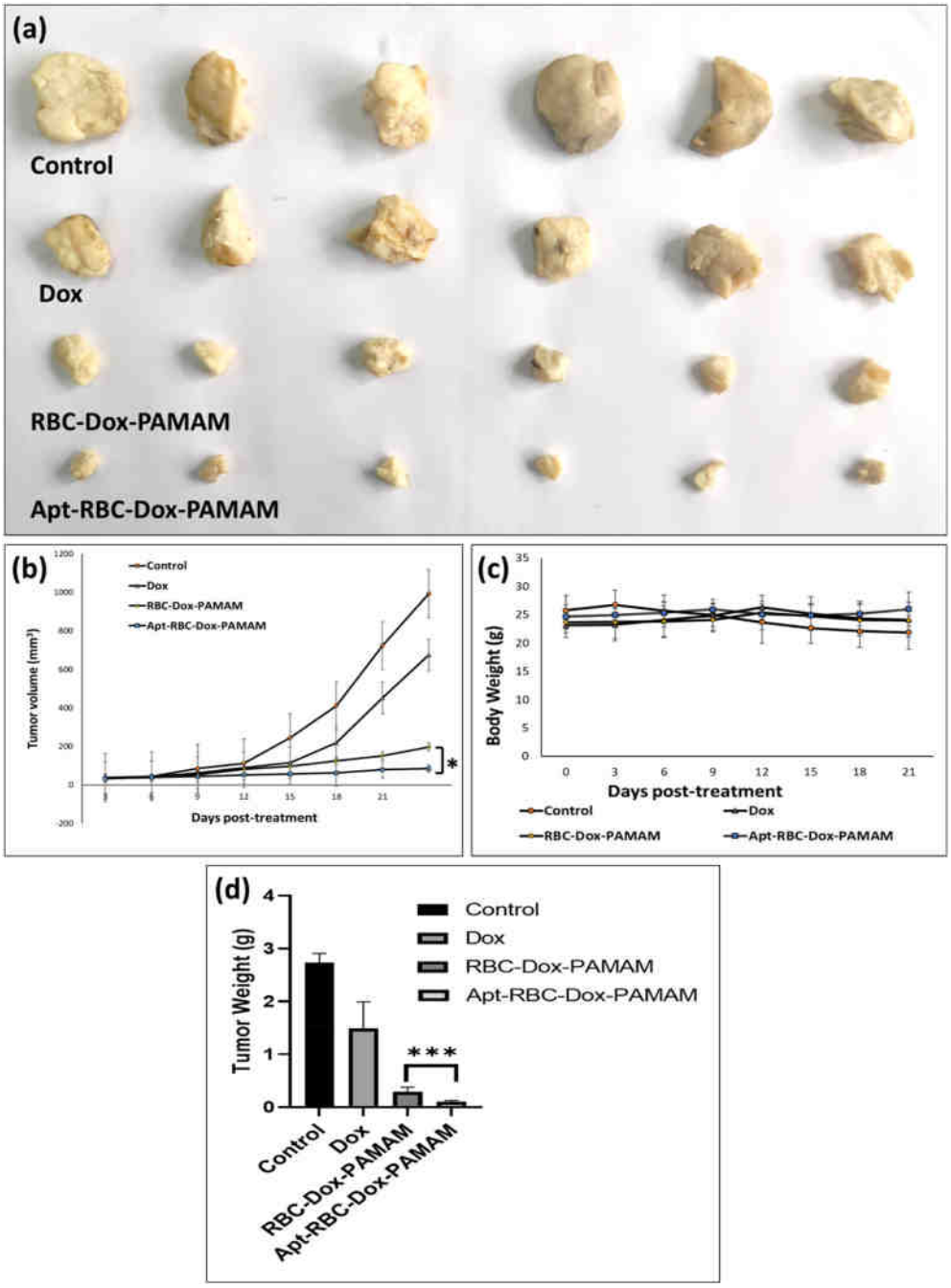

Fig. 9. Antitumor efficacy of Apt-RBC-Dox-PAMAM in 4T1-bearing mice model. Pattern of tumor growth in 4T1-bearing mice model (a and b) receiving in intravenous dose of Dox, RBC-Dox-PAMAM and Apt-RBC-Dox-PAMAM; representation of changes in the body weight in 4T1-tumorized mice model post-treatment with Dox, RBC-Dox-PAMAM and Apt-RBC-Dox-PAMAM (c), tumor weight of mice post-treatment with various samples (d) [* represents $p < 0.05$, *** represents $p < 0.001$].

mice receiving 5 mg/kg equivalent amount of Dox. An appreciable tumor inhibitory effect was observed by the formulations as compared with the free drug. An elevated effect of RBC-Dox-PAMAM on tumor-bearing mice model over those treated with free drug owes to the enhanced permeation and retention (EPR) effect leading to higher accumulation of therapeutic cargo. The coating of RBC membrane on PAMAM dendrimers extended the circulation time that delayed the early clearance of the drug from the bloodstream. A superior tumor inhibitory effect of Apt-RBC-Dox-PAMAM over non-targeted therapy was observed, which is due to higher internalization through receptor-mediated endocytosis. The selectivity of EpCAM aptamer towards EpCAM-positive tumor cells also facilitated improved tumor residence time, decreasing its extravasation. Note that most of the cancer cells failed to show effective results due to resistance to certain chemotherapy. The reason could be tumor heterogeneity or Pg-p efflux. The receptor-mediated response could overcome such hurdles by escaping endosomal uptake. All such stated responsible features improved the therapeutic potential of aptamer-based therapy over non-targeted therapy (Fig. 9a and b).

We further examined the treatment's toxicity and safety by analyzing the effect on body weight loss (Fig. 9c). No considerable weight loss was observed post-administration of treatment with targeted preparation that confirmed its non-toxicity, adequate dosage, and safe treatment regimen. Such a finding confirms the enhanced therapeutic response of

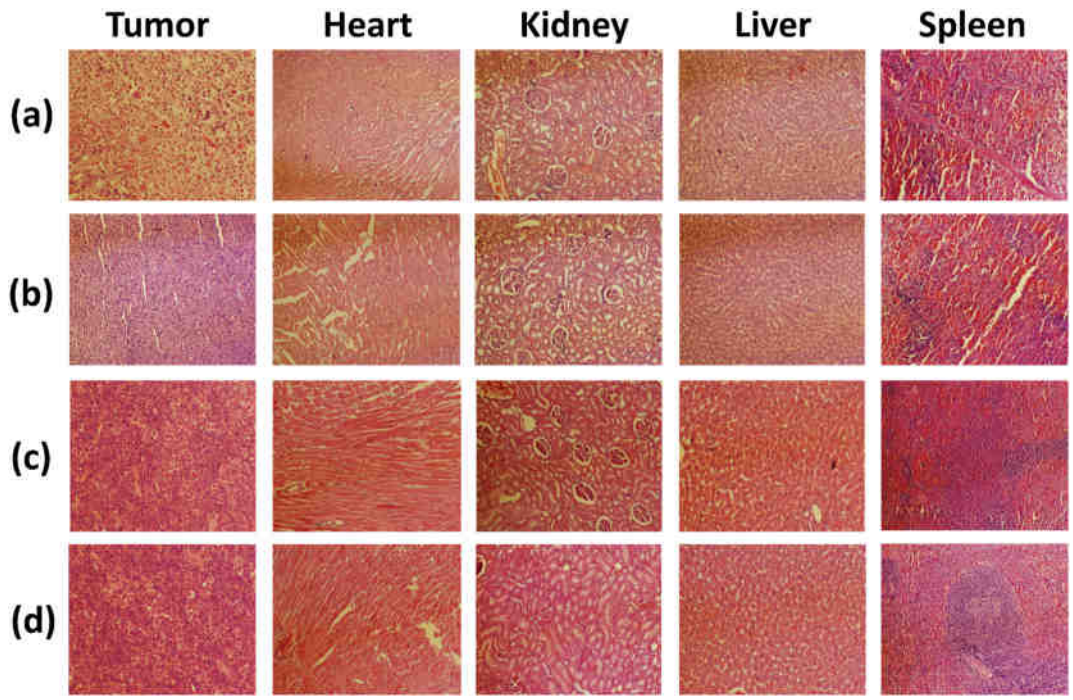

Fig. 10. Representation of hematoxylin and eosin-stained tissue of major organ and tumor tissue of 4T1-laden mice post-treatment with control (a), Dox (b), RBC-Dox-PAMAM (c) and Apt-RBC-Dox-PAMAM (d).

aptamer-functionalized drug delivery systems. Fig. 9d demonstrates the tumor weight of mice after treatment, confirming that Apt-RBC-Dox-PAMAM has superior tumor suppressive effect *in vivo*.

3.7. Pathological evaluation of systemic toxicity

Nanotechnology has paved the way in cancer treatment; however, it can affect the physiology of normal cells as well lead to increased toxic effects and organ failure. To overcome such issues, targeted drug delivery systems came into the limelight promoting selective uptake by the tumor cells only without affecting the normal cells. Aptamer-based targeted therapy potentiated increased uptake which resulted in a higher accumulation of drug at the site of action. Apart from therapeutic response, the success of therapy is also a response to its non-toxic effects on vital organs. To establish this, major organs on mice were extracted and pathological alterations of tumors and organs were examined (Fig. 10). A high degree of tumor necrosis was observed in mice treated with Apt-RBC-Dox-PAMAM in comparison to those treated with non-targeted therapy and plain Dox, indicating a superior anticancer effect. High chromatin ratio and large nuclei were observed in the group treated with plain drug and PBS, demonstrating the cell proliferation capability of cancer cells. It is worth mentioning here that, the heart tissue of mice showed severe pathological injuries after treatment with free Dox; however, no histological alterations were reported in those treated with RBC-Dox-PAMAM and Apt-RBC-Dox-PAMAM. This is due to the EPR effect and cell response to non-targeted and targeted preparations, confirming the success of therapy when delivered via PAMAM dendrimers [67].

4. Conclusion

In summary, we developed a cell membrane-camouflaged nano-oncotherapeutic system by coating Dox-loaded PAMAM dendrimers with the RBC membrane. To improve the tumor selectivity and cellular internalization, an EpCAM aptamer was conjugated on the surface of RBC-Dox-PAMAM. The enveloped novel drug delivery system improved the blood circulation time while sensitizing the EpCAM-positive tumor cells to onco-therapeutics to provide the utmost therapeutic effect. The *in vivo* investigation on 4T1-laden tumor mice model demonstrated a significant tumor suppressive effect. The results obtained suggested that the developed targeted biomimetic therapy could improve the clinical outcome and survival of mice with TNBC.

Ethics statement

The *in vivo* antitumor study was carried out in female Balb/c mice after approval from the institutional animal ethics committee (Protocol no. 1734).

Credit author statement

All the authors have been contributed significantly and equally to complete this manuscript.

Declaration of competing interest

The authors declare that they have no known competing financial interests or personal relationships that could have appeared to influence the work reported in this paper.

Data availability

Data will be made available on request.

Acknowledgments

Author (Alaa S. Tulbah) would like to thank the Deanship of Scientific Research at Umm Al-Qura University for supporting this work by grant code (23UQU4280449DSR003). The authors would like to acknowledge the Indian Council of Medical Research (ICMR) for providing fellowship to Afsana (fellowship ID 3/2/2/68/2022/NCD-III) and Department of Science and Technology (DST) for providing financial assistance under FIST Programme, respectively to the department of pharmaceutics, SPER, Jamia Hamdard. The author (P. Kesharwani)

acknowledges the financial support from the Indian Council of Medical Research (ICMR), New Delhi, India, through Extramural Research Grants [35/10/2019-Nano/BMS and 5/August 13, 2020/NCDIII].

References

[1] K.A. Won, C. Spruck, Triple-negative breast cancer therapy: current and future perspectives, Int. J. Oncol. 57 (2020) 1245, https://doi.org/10.3892/IJO.2020.5135.

[2] Z. Mirza, S. Karim, Nanoparticles-based drug delivery and gene therapy for breast cancer: recent advancements and future challenges, Semin. Cancer Biol. 69 (2021) 226–237, https://doi.org/10.1016/J.SEMCANCER.2019.10.020.

[3] L. Yin, J.J. Duan, X.W. Bian, S.C. Yu, Triple-negative breast cancer molecular subtyping and treatment progress, Breast Cancer Res. 22 (2020) 1–13, https://doi.org/10.1186/s13058-020-01296-5.

[4] W. Qin, J. Chandra, M.A.S. Abourehab, N. Gupta, Z.S. Chen, P. Kesharwani, H. L. Cao, New opportunities for RGD-engineered metal nanoparticles in cancer, Mol. Cancer 22 (2023) 87, https://doi.org/10.1186/S12943-023-01784-0/FIGURES/8.

[5] L. Zeng, B.H.J. Gowda, M.G. Ahmed, M.A.S. Abourehab, Z.S. Chen, C. Zhang, J. Li, P. Kesharwani, Advancements in nanoparticle-based treatment approaches for skin cancer therapy, Mol. Cancer (2023) 1–50, https://doi.org/10.1186/S12943-022-01708-4, 2023 221. 22.

[6] Z. Liu, N. Parveen, U. Rehman, A. Aziz, A. Sheikh, M.A.S. Abourehab, W. Guo, J. Huang, Z. Wang, P. Kesharwani, Unravelling the enigma of siRNA and aptamer mediated therapies against pancreatic cancer, Mol. Cancer (2023) 1–22, https://doi.org/10.1186/S12943-022-01696-5, 2023 221. 22.

[7] M. Fatima Sristi, A. Sheikh, W.H. Almalki, S. Talegaonkar, S.K. Dubey, M.C.I. M. Amin, A. Sahebkar, P. Kesharwani, Recent Advancement on Albumin Nanoparticles in Treating Lung Carcinoma, 2023, pp. 486–499, https://doi.org/10.1080/1061186X.2023.2205609. Https://Doi.Org/10.1080/1061186X.2023.2205609. 31.

[8] J. Ahamed, B.H. Jaswanth Gowda, W.H. Almalki, N. Gupta, A. Sahebkar, P. Kesharwani, Recent advances in nanoparticle-based approaches for the treatment of brain tumors: opportunities and challenges, Eur. Polym. J. 193 (2023), 112111, https://doi.org/10.1016/J.EURPOLYMJ.2023.112111.

[9] S.A. Torres-Pérez, M. del P. Ramos-Godínez, E. Ramón-Gallegos, Glycosylated one-step PAMAM dendrimers loaded with methotrexate for target therapy in breast cancer cells MDA-MB-231, J. Drug Deliv. Sci. Technol. (2020), 101769, https://doi.org/10.1016/j.jddst.2020.101769.

[10] A. Sneider, R. Jadia, B. Piel, D. VanDyke, C. Tsiros, P. Rai, Engineering remotely triggered liposomes to target triple negative breast cancer, Oncomedicine 2 (2017) 1, https://doi.org/10.7150/ONCM.17406.

[11] D. Sharma, S. Singh, P. Kumar, G.K. Jain, G. Aggarwal, W.H. Almalki, P. Kesharwani, Mechanisms of photodynamic therapy, Nanomater. Photodyn. Ther. (2023) 41–54, https://doi.org/10.1016/B978-0-323-85595-2.00017-7.

[12] M. Fatima, R. Karwasra, W.H. Almalki, A. Sahebkar, P. Kesharwani, Galactose engineered nanocarriers: hopes and hypes in cancer therapy, Eur. Polym. J. 183 (2023), 111759, https://doi.org/10.1016/J.EURPOLYMJ.2022.111759.

[13] P. Falagan-Lotsch, E.M. Grzincic, C.J. Murphy, New advances in nanotechnology-based diagnosis and therapeutics for breast cancer: an assessment of active-targeting inorganic nanoplatforms, Bioconjugate Chem. 28 (2017) 135–152, https://doi.org/10.1021/ACS.BIOCONJCHEM.6B00591.

[14] K. Greish, A. Mathur, R. Al Zahrani, S. Elkaissi, M. Al Jishi, O. Nazzal, S. Taha, V. Pittalà, S. Taurin, Synthetic cannabinoids nano-micelles for the management of triple negative breast cancer, J. Contr. Release (2018), https://doi.org/10.1016/j.jconrel.2018.10.030.

[15] X. Jin, Y. Wei, F. Xu, M. Zhao, K. Dai, R. Shen, S. Yang, N. Zhang, SIRT1 promotes formation of breast cancer through modulating Akt activity, J. Cancer 9 (2018) 2012, https://doi.org/10.7150/JCA.24275.

[16] N. Parveen, A. Sheikh, M.A.S. Abourehab, R. Karwasra, S. Singh, P. Kesharwani, Self-nanoemulsifying drug delivery system for pancreatic cancer, Eur. Polym. J. 190 (2023), 111993, https://doi.org/10.1016/J.EURPOLYMJ.2023.111993.

[17] T.T. Dongsar, T.S. Dongsar, M.A.S. Abourehab, N. Gupta, P. Kesharwani, Emerging application of magnetic nanoparticles for breast cancer therapy, Eur. Polym. J. 187 (2023), 111898, https://doi.org/10.1016/J.EURPOLYMJ.2023.111898.

[18] P. Kesharwani, A. Sheikh, M.A.S. Abourehab, R. Salve, V. Gajbhiye, A combinatorial delivery of survivin targeted siRNA using cancer selective nanoparticles for triple negative breast cancer therapy, J. Drug Deliv. Sci. Technol. 80 (2023), 104164, https://doi.org/10.1016/J.JDDST.2023.104164.

[19] N. Parveen, M.A.S. Abourehab, R. Shukla, P.V. Thanikachalam, G.K. Jain, P. Kesharwani, Immunoliposomes as an emerging nanocarrier for breast cancer therapy, Eur. Polym. J. 184 (2023), 111781, https://doi.org/10.1016/J.EURPOLYMJ.2022.111781.

[20] T.T. Dongsar, T.S. Dongsar, N. Gupta, W.H. Almalki, A. Sahebkar, P. Kesharwani, Emerging potential of 5-Fluorouracil-loaded chitosan nanoparticles in cancer therapy, J. Drug Deliv. Sci. Technol. 82 (2023), 104371, https://doi.org/10.1016/J.JDDST.2023.104371.

[21] D.A. Tomalia, H. Baker, J. Dewald, M. Hall, G. Kallos, S. Martin, J. Roeck, J. Ryder, P. Smith, A New class of polymers: starburst-dendritic macromolecules, Polym. J. 17 (1985) 117–132, https://doi.org/10.1295/polymj.17.117.

[22] P. Kesharwani, R.K. Tekade, N.K. Jain, Dendrimer generational nomenclature: the need to harmonize, Drug Discov. Today 20 (2015), https://doi.org/10.1016/j.drudis.2014.12.015.

[23] P. Kesharwani, K. Jain, N.K. Jain, Dendrimer as nanocarrier for drug delivery, Prog. Polym. Sci. 39 (2014) 268–307, https://doi.org/10.1016/j.progpolymsci.2013.07.005.

[24] A. Sheikh, S. Md, P. Kesharwani, RGD engineered dendrimer nanotherapeutic as an emerging targeted approach in cancer therapy, J. Contr. Release 340 (2021) 221–242, https://doi.org/10.1016/J.JCONREL.2021.10.028.

[25] P. Kesharwani, V. Gajbhiye, N.K. Jain, A review of nanocarriers for the delivery of small interfering RNA, Biomaterials 33 (2012) 7138–7150, https://doi.org/10.1016/j.biomaterials.2012.06.068.

[26] T. Il Kim, H.J. Seo, J.S. Choi, H.S. Jang, J.U. Baek, K. Kim, J.S. Park, Pamam-Peg-Pamam, Novel triblock copolymer as a biocompatible and efficient gene delivery carrier, Biomacromolecules 5 (2004) 2487–2492, https://doi.org/10.1021/bm049563j.

[27] J. Li, Y. Han, Y. Lu, B. Song, M. Zhao, H. Hu, D. Chen, A novel disulfide bond-mediated cleavable RGD-modified PAMAM nanocomplex containing nuclear localization signal HMGB1 for enhancing gene transfection efficiency, Int. J. Nanomed. 13 (2018) 7135–7153, https://doi.org/10.2147/IJN.S182445.

[28] P. Kesharwani, L. Xie, G. Mao, S. Padhye, A.K. Iyer, Hyaluronic Acid-Conjugated Polyamidoamine Dendrimers for Targeted Delivery of 3,4-difluorobenzylidene Curcumin to CD44 Overexpressing Pancreatic Cancer Cells, vol. 136, 2015, pp. 413–423, https://doi.org/10.1016/j.colsurfb.2015.09.043.

[29] S. Wen, H. Liu, H. Cai, M. Shen, X. Shi, Targeted and pH-responsive delivery of doxorubicin to cancer cells using multifunctional dendrimer-modified multi-walled carbon nanotubes, Adv. Healthc. Mater. 2 (2013) 1267–1276, https://doi.org/10.1002/adhm.201200389.

[30] H. Yao, J. Ma, Dendrimer-paclitaxel complexes for efficient treatment in ovarian cancer: study on OVCAR-3 and HEK293T cells, Acta Biochim. Pol. 65 (2018) 219–225, https://doi.org/10.18388/abp.2017_2331.

[31] J.B. Otis, H. Zong, A. Kotylar, A. Yin, S. Bhattacharjee, H. Wang, J.R. Baker, S. H. Wang, Dendrimer antibody conjugate to target and image HER-2 overexpressing cancer cells, Oncotarget 7 (2016) 36002–36013, https://doi.org/10.18632/oncotarget.9081.

[32] H. Dong, L. Han, J. Wang, J. Xie, Y. Gao, F. Xie, L. Jia, In vivo inhibition of circulating tumor cells by two apoptosis-promoting circular aptamers with enhanced specificity, J. Contr. Release 280 (2018) 99–112, https://doi.org/10.1016/j.jconrel.2018.05.004.

[33] M. Ghaffari, G. Dehghan, B. Baradaran, A. Zarebkohan, B. Mansoori, J. Soleymani, J. Ezzati Nazhad Dolatabadi, M.R. Hamblin, Co-delivery of curcumin and Bcl-2 siRNA by PAMAM dendrimers for enhancement of the therapeutic efficacy in HeLa cancer cells, Colloids Surf. B Biointerfaces 188 (2020), 110762, https://doi.org/10.1016/j.colsurfb.2019.110762.

[34] J. Czarnik-Kwaśniak, K. Kwaśniak, K. Tutaj, I. Filiks, Ł. Uram, M. Stompor, S. Wołowiec, Glucoheptoamidated polyamidoamine PAMAM G3 dendrimer as a vehicle for succinate linked doxorubicin; enhanced toxicity of DOX against grade IV glioblastoma U-118 MG cells, J. Drug Deliv. Sci. Technol. 55 (2020), 101424, https://doi.org/10.1016/j.jddst.2019.101424.

[35] M. K, K. S, P. N, L. V, P. D, Dendrimers in drug delivery and targeting: drug-dendrimer interactions and toxicity issues, J. Pharm. BioAllied Sci. 6 (2014) 139–150, https://doi.org/10.4103/0975-7406.130965.

[36] N. Malavia, R. Ghadi, K. Kuche, T. Date, N. Bhargavi, D. Chaudhari, R. Swami, P. B. Katare, S.K. Banerjee, S. Jain, Green surfactant-dendrimer aggreplexes: an ingenious way to launch dual attack on arch-enemy cancer, Colloids Surf. B Biointerfaces 204 (2021), 111821, https://doi.org/10.1016/j.colsurfb.2021.111821.

[37] S.T. Kumbhar, R.Y. Patil, M.S. Bhatia, P.B. Choudhari, V.L. Gaikwad, Synthesis and characterization of chitosan nanoparticles decorated with folate and loaded with dasatinib for targeting folate receptors in cancer cells, Open 7 (2022), 100043, https://doi.org/10.1016/J.ONANO.2022.100043.

[38] B. Gorain, M. Pandey, H. Choudhury, G.K. Jain, P. Kesharwani, Dendrimer for solubility enhancement, in: Dendrimer-Based Nanotherapeutics, Elsevier, 2021, pp. 273–283, https://doi.org/10.1016/B978-0-12-821250-9.00025-1.

[39] C.M.J. Hu, R.H. Fang, B.T. Luk, L. Zhang, Polymeric nanotherapeutics: clinical development and advances in stealth functionalization strategies, Nanoscale 6 (2014) 65–75, https://doi.org/10.1039/C3NR05444F.

[40] Z. Zhang, H. Qian, M. Yang, R. Li, J. Hu, L. Li, L. Yu, B. Liu, X. Qian, Gambogic acid-loaded biomimetic nanoparticles in colorectal cancer treatment, Int. J. Nanomed. 12 (2017) 1593, https://doi.org/10.2147/IJN.S127256.

[41] A. Sheikh, P. Kesharwani, An insight into aptamer engineered dendrimer for cancer therapy, Eur. Polym. J. 159 (2021), 110746, https://doi.org/10.1016/J.EURPOLYMJ.2021.110746.

[42] G. Gastl, G. Spizzo, P. Obrist, M. Dünser, G. Mikuz, Ep-CAM overexpression in breast cancer as a predictor of survival, Lancet 356 (2000) 1981–1982, https://doi.org/10.1016/S0140-6736(00)03312-2 (London, England).

[43] A. Gilboa-Geffen, P. Hamar, M.T.N. Le, L.A. Wheeler, R. Trifonova, F. Petrocca, A. Wittrup, J. Lieberman, Gene knockdown by EpCAM aptamer-siRNA chimeras suppresses epithelial breast cancers and their tumor-initiating cells, Mol. Cancer Therapeut. 14 (2015) 2279–2291, https://doi.org/10.1158/1535-7163.MCT-15-0201-T/85497/AM/GENE-KNOCKDOWN-BY-EPCAM-APTAMER-SIRNA-CHIMERAS.

[44] M. Mohammadi, Z. Salmasi, M. Hashemi, F. Mosaffa, K. Abnous, M. Ramezani, Single-walled carbon nanotubes functionalized with aptamer and piperazine-polyethylenimine derivative for targeted siRNA delivery into breast cancer cells, Int. J. Pharm. 485 (2015) 50–60, https://doi.org/10.1016/J.IJPHARM.2015.02.031.

[45] H.J. Zhang, X. Zhao, L.J. Chen, C.X. Yang, X.P. Yan, Dendrimer grafted persistent luminescent nanoplatform for aptamer guided tumor imaging and acid-responsive

drug delivery, Talanta 219 (2020), 121209, https://doi.org/10.1016/j.talanta.2020.121209.
[46] Y. Wang, C. Zhou, Y. Ding, M. Liu, Z. Tai, Q. Jin, Y. Yang, Z. Li, M. Yang, W. Gong, C. Gao, Red blood cell-hitchhiking chitosan nanoparticles for prolonged blood circulation time of vitamin K1, Int. J. Pharm. 592 (2021), 120084, https://doi.org/10.1016/j.ijpharm.2020.120084.
[47] Y. Guo, D. Wang, Q. Song, T. Wu, X. Zhuang, Y. Bao, M. Kong, Y. Qi, S. Tan, Z. Zhang, Erythrocyte membrane-enveloped polymeric nanoparticles as nanovaccine for induction of antitumor immunity against melanoma, ACS Nano 9 (2015) 6918–6933, https://doi.org/10.1021/acsnano.5b01042.
[48] M. P, C. R A, G. S M, B.-R. A, A. M S, AS1411 aptamer-anionic linear globular dendrimer G2-iohexol selective nano-theranostics, Sci. Rep. 7 (2017), 11832.
[49] A. Barzegar Behrooz, F. Nabavizadeh, J. Adiban, M. Shafiee Ardestani, R. Vahabpour, M.R. Aghasadeghi, H. Sohanaki, Smart bomb AS1411 aptamer-functionalized/PAMAM dendrimer nanocarriers for targeted drug delivery in the treatment of gastric cancer, Clin. Exp. Pharmacol. Physiol. 44 (2017) 41–51, https://doi.org/10.1111/1440-1681.12670.
[50] P.K. Tripathi, B. Gorain, H. Choudhury, A. Srivastava, P. Kesharwani, Dendrimer entrapped microsponge gel of dithranol for effective topical treatment, Heliyon 5 (2019), https://doi.org/10.1016/j.heliyon.2019.e01343.
[51] X. Yang, L. Wang, L. Li, M. Han, S. Tang, T. Wang, J. Han, X. He, X. He, A. Wang, K. Sun, A novel dendrimer-based complex co-modified with cyclic RGD hexapeptide and penetratin for noninvasive targeting and penetration of the ocular posterior segment, Drug Deliv. 26 (2019) 989–1001, https://doi.org/10.1080/10717544.2019.1667455.
[52] I.H. Lee, S. An, M.K. Yu, H.K. Kwon, S.H. Im, S. Jon, Targeted chemoimmunotherapy using drug-loaded aptamer-dendrimer bioconjugates, J. Contr. Release 155 (2011) 435–441, https://doi.org/10.1016/j.jconrel.2011.05.025.
[53] P. Kesharwani, S. Banerjee, S. Padhye, F.H. Sarkar, A.K. Iyer, Hyaluronic acid engineered nanomicelles loaded with 3,4-difluorobenzylidene curcumin for targeted killing of CD44+ stem-like pancreatic cancer cells, Biomacromolecules 16 (2015), https://doi.org/10.1021/acs.biomac.5b00941.
[54] P. Kesharwani, L. Xie, S. Banerjee, G. Mao, S. Padhye, F.H. Sarkar, A.K. Iyer, Hyaluronic acid-conjugated polyamidoamine dendrimers for targeted delivery of 3,4-difluorobenzylidene curcumin to CD44 overexpressing pancreatic cancer cells, Colloids Surf. B Biointerfaces 136 (2015) 413–423, https://doi.org/10.1016/j.colsurfb.2015.09.043.
[55] M. Shahriari, S.M. Taghdisi, K. Abnous, M. Ramezani, M. Alibolandi, Synthesis of hyaluronic acid-based polymersomes for doxorubicin delivery to metastatic breast cancer, Int. J. Pharm. 572 (2019), 118835, https://doi.org/10.1016/j.ijpharm.2019.118835.
[56] C.M. Pinto, L.S. Horta, A.P. Soares, B.A. Carvalho, E. Ferreira, E.B. Lages, L.A. M. Ferreira, A.A.G. Faraco, H.C. Santiago, G.A.C. Goulart, Nanoencapsulated doxorubicin prevents mucositis development in mice, Pharmaceutics 13 (2021), https://doi.org/10.3390/pharmaceutics13071021.
[57] J. Zhu, Z. Xiong, M. Shen, X. Shi, Encapsulation of doxorubicin within multifunctional gadolinium-loaded dendrimer nanocomplexes for targeted theranostics of cancer cells, RSC Adv. 5 (2015) 30286–30296, https://doi.org/10.1039/c5ra01215e.
[58] A. Rudra, R.M. Deepa, M.K. Ghosh, S. Ghosh, B. Mukherjee, Doxorubicin-loaded phosphatidylethanolamine-conjugated nanoliposomes: in vitro characterization and their accumulation in liver, kidneys, and lungs in rats, Int. J. Nanomed. 5 (2010) 811–823, https://doi.org/10.2147/IJN.S13031.
[59] S. Li, Y. Ma, X. Yue, Z. Cao, Z. Dai, One-pot construction of doxorubicin conjugated magnetic silica nanoparticles, New J. Chem. 33 (2009) 2414–2418, https://doi.org/10.1039/B9NJ00342H.
[60] D.H. Nguyen, L.G. Bach, D.H.N. Tran, V. Du Cao, T.N.Q. Nguyen, T.T.H. Le, T. T. Tran, T.T.H. Thi, Partial surface modification of low generation polyamidoamine dendrimers: gaining insight into their potential for improved carboplatin delivery, Biomolecules 9 (2019) 1–16, https://doi.org/10.3390/biom9060214.
[61] I. Khan, G. Joshi, K.T. Nakhate, Ajazuddin, R. Kumar, U. Gupta, Nano-Co-Delivery of berberine and anticancer drug using PLGA nanoparticles: exploration of better anticancer activity and in vivo kinetics, Pharm. Res. (N. Y.) 36 (2019), https://doi.org/10.1007/s11095-019-2677-5.
[62] M. Alibolandi, F. Hoseini, M. Mohammadi, P. Ramezani, E. Einafshar, S. M. Taghdisi, M. Ramezani, K. Abnous, Curcumin-entrapped MUC-1 aptamer targeted dendrimer-gold hybrid nanostructure as a theranostic system for colon adenocarcinoma, Int. J. Pharm. 549 (2018) 67–75, https://doi.org/10.1016/j.ijpharm.2018.07.052.
[63] M. Alibolandi, M. Ramezani, F. Sadeghi, K. Abnous, F. Hadizadeh, Epithelial cell adhesion molecule aptamer conjugated PEG-PLGA nanopolymersomes for targeted delivery of doxorubicin to human breast adenocarcinoma cell line in vitro, Int. J. Pharm. 479 (2015) 241–251, https://doi.org/10.1016/j.ijpharm.2014.12.035.
[64] M. Alibolandi, M. Ramezani, K. Abnous, F. Hadizadeh, AS1411 aptamer-decorated biodegradable polyethylene glycol–poly(lactic-co-glycolic acid) nanopolymersomes for the targeted delivery of gemcitabine to non–small cell lung cancer in vitro, J. Pharmaceut. Sci. 105 (2016) 1741–1750, https://doi.org/10.1016/J.XPHS.2016.02.021.
[65] M. Falsafi, M. Zahiri, A.S. Saljooghi, K. Abnous, S.M. Taghdisi, A. Sazgarnia, M. Ramezani, M. Alibolandi, Aptamer targeted red blood cell membrane-coated porphyrinic copper-based MOF for guided photochemotherapy against metastatic breast cancer, Microporous Mesoporous Mater. 325 (2021), 111337, https://doi.org/10.1016/j.micromeso.2021.111337.
[66] X. Xu, L. Li, X. Li, D. Tao, P. Zhang, J. Gong, Aptamer-protamine-siRNA nanoparticles in targeted therapy of ErbB3 positive breast cancer cells, Int. J. Pharm. 590 (2020), https://doi.org/10.1016/j.ijpharm.2020.119963.
[67] M. Mohammadi, L. Arabi, M. Alibolandi, Doxorubicin-loaded composite nanogels for cancer treatment, J. Contr. Release 328 (2020) 171–191, https://doi.org/10.1016/j.jconrel.2020.08.033.

Environmental Research 234 (2023) 116562

Contents lists available at ScienceDirect

Environmental Research

journal homepage: www.elsevier.com/locate/envres

Self-assembled Gallic acid loaded lecithin-chitosan hybrid nanostructured gel as a potential tool against imiquimod-induced psoriasis

Sahim Aziz Hazari [a], Afsana Sheikh [a], Mohammed A.S. Abourehab [b,c], Alaa S. Tulbah [c], Prashant Kesharwani [a,d,1,*]

[a] Department of Pharmaceutics, School of Pharmaceutical Education and Research, Jamia Hamdard, New Delhi, 110062, India
[b] Department of Pharmaceutics and Industrial Pharmacy, College of Pharmacy, Minia University, Minia, 61519, Egypt
[c] Pharmaceutics Department, College of Pharmacy, Umm Al Qura University, Makkah, Saudi Arabia
[d] Department of Pharmacology, Saveetha Dental College, Saveetha Institute of Medical and Technical Sciences, Saveetha University, Chennai, India

ARTICLE INFO

Keywords:
Psoriasis
Gallic acid
Lipid-hybrid nanoparticles
Topical delivery
Nanomedicine

ABSTRACT

Increased thickness of the skin and hyperproliferation of keratinocyte cell is the main obstacle in the treatment of psoriasis. Gallic Acid (GA) has shown efficacious results against the hyperproliferation of keratinocytes while lipid-polymer loaded hybrid nanoparticles (LPHNs) have an edge over lipidic and polymeric nanoparticles considering drug loading, controlled release, stability, and retention. The LPHNs were optimized using Box-Behnken method and was further characterized by FTIR, DSC and Zetasizer. The optimized preparation demonstrated a size of 170.5 ± 0.087 nm and a PDI of 0.19 ± 0.0015, respectively. The confocal study has suggested that the hybrid nanosystem enhanced the drug penetration into the deeper layer with a higher drug release of 79 ± 0.001% as compared to the gallic acid-loaded gel. In addition, the formulation significantly reduced PASI score and splenomegaly without causing any serious irritation. The morphological study of the spleen suggested that the prepared formulation has well controlled the disease compared to the marketed formulation while maintaining a normal level of immune cells after treatment. Hence GALPHN could be accepted as one of the excellent vehicles for the topical conveyance of GA (gallic acid) due to enhanced penetration, and good retention, along with fewer side effects and higher efficacy of the GALPHN gel against imiquimod (IMQ) induced psoriasis.

1. Introduction

Psoriasis is a chronic, immune-mediated disorder that affects the outlook of the epidermal layer making them flaky, patchy, and appearance of scales. The keratinocytes could hardly be differentiated causing cell proliferation (Rachakonda et al., 2014). Starting from a single spot, it can spread to the whole body leading to severe inflammation and plaque on the skin (Tambe et al., 2021). It has tremendously affected Western countries as compared to other parts of the world. Nearly, 2–4% of the world population has been affected by the lifelong immune-mediated disease, thus giving anti-psoriatic agents a market of 18 billion USD in the year 2021 (Ali et al., 2019; "Plaque Psoriasis). Fortunately, psoriasis is not lethal or life-threatening, however, it does reduce one's quality of life making the patient susceptible to numerous comorbidities (Aldredge and Higham, 2018) as diabetes, psoriatic arthritis, cardiac disorders, hyperlipidaemia, peptic ulcer, metabolic disorders, and so on (Chen et al., 2022). Immune cells for say Interleukin-17 (IL-17), IL-6 CD44, APC, IL-37, IL-22, Interferon (INF)-γ and Tumor necrosis factor (TNF)-α, etc are overexpressed in psoriasis. Such overexpression of immune cells is the major cause of inflammation in diseased conditions (Kang et al., 2018). Any part of the skin can be affected by psoriasis but generally, it begins from particular sites such as the knees, groin, scalp, etc.

No permanent cure for psoriasis is available now for psoriasis as most of the treatments available are based on symptoms and come with severe side effects on long-term use (Psoriasis Treatments). Some of the effective treatments available against psoriasis are calcitriol, steroids, calcineurin inhibitor, tacrolimus, etc, However, they only provide symptomatic relief by interacting with the patient's immune cells, causing severe side effects and making the individual more susceptible

* Corresponding author. Department of Pharmaceutics, School of Pharmaceutical Education and Research, Jamia Hamdard, New Delhi, 110062, India.
E-mail address: prashantdops@gmail.com (P. Kesharwani).
[1] https://scholar.google.com/citations?user=DJkvOAQAAAAJ&hl=en.

https://doi.org/10.1016/j.envres.2023.116562
Received 5 June 2023; Received in revised form 26 June 2023; Accepted 4 July 2023
Available online 5 July 2023

to other diseases (Ghate et al., 2019). There are various routes to deliver the drug but the use of inappropriate routes may reduce the disposition of the drug at the site and increase the side effects (Rahman et al., 2012). The topical route is one of the choices for the treatment of psoriasis as a drug can be delivered to specific sites with reduced toxicity. However, the most important stumbling block in skin physiology is the rigidness and cell permeability (Pinto et al., 2014) due to keratinocyte hyper-proliferation and rapid degeneration resulting in low bioavailability and disposition of cargoes in the lower epidermis (Parveen et al., 2023b; Pradhan et al., 2021). The disadvantages of presently accessible standard treatment could be eliminated by encapsulating drugs in nanoparticles, which will improve permeation while decreasing toxicity. Surface modifications of nanoparticles improve the retention of the drug at the required site (Ahamed et al., 2023; Dongsar et al., 2023b; Jagdale et al., 2023; Kesharwani et al., 2014; Liu et al., 2023; Parveen et al., 2023a; Pukale et al., 2020; Zeng et al., 2023).

Processed beverages, e.g., green tea, and red wines, are rich sources of Gallic acid (GA) or (3, 4, 5-tri hydroxybenzoic acid), which is a natural polyphenolic compound. It can be extracted from various sources from all over the plant kingdoms, including roots, leaves, and bark (gall nuts and pomegranates). Caffeic acid or trihydroxy cinnamic acid can be used to synthesize it from phenylalanine. Gallic acid is recognized for its potent antioxidative, anticarcinogenic, antimutagenic, antiallergic, antiviral, anti-inflammatory, antibacterial and anti-arteriosclerosis, anti-proliferative, Nrf2 gene suppression, anti-psoriatic activities (Choubey et al., 2015). Although, poor bioavailability through the topical route is a major drawback. The development of nanocarriers may alleviate the constituents' poor bioavailability via topical and transdermal routes (Choubey et al., 2015; Zhang et al., 2018).

Nanotechnology is a breakthrough in medical field considering lower side effects, low dose, site specificity and improved therapeutic applicability (Aziz Hazari et al., 2023; Fiedler et al., 2023; Islam et al., 2022; Karimi-Maleh et al., 2023). Nanoparticles have continuously been explored in the treatment of various diseases like skin cancer, breast cancer, psoriasis, wound healing, neurological diseases, osteoporosis and general fungal diseases etc (Cassano et al., 2021; Gavas et al., 2021; Gupta et al., 2022; Gyanewali et al., 2021; Kesharwani et al., 2023). Use of nanoparticles in cancer, fungal or bacterial diseases has reduced the dose and side effects of anticancer drugs due to the site specific drug release (Ganesan et al., 2021; Renzi et al., 2021), while skin diseases such as psoriasis and dermatitis can be treated by overcoming the delivery barriers through enhance permeation and retention of nanoparticles (Xi et al., 2022).

Along with all the benefits of nanoparticles based on lipids, there are some drawbacks in terms of encapsulation efficiency and stability that could be mitigated by preparing hybrid nanoparticles by combining polymer and lipid, having benefits of both polymeric and lipid-based nanoparticles to the newly formed hybrid nanoparticle (Akentieva et al., 2020; Aziz et al., 2022; Dongsar et al., 2023a; Fatima et al., 2023; Hamdi et al., 2022; Kesharwani et al., 2023; Pramual et al., 2017; Zhao et al., 2023). Hybrid nanoparticles are modified nanoparticles that can be formed by conjugation of polymer-polymer, lipid-polymer, etc. According to the purpose, which provides more stability, more targetability, more penetration, and other advantages depending on the rationale-oriented modification (Pukale et al., 2020).

Chitosan is a naturally occurring polysaccharide composed of glucosamine copolymers and N-acetyl- glucosamine units linked by β-1,4-glycosidic linkages (Ashrafizadeh et al., 2020, 2021, 2023). It has structural similarity with the extracellular matrix, exceptional biocompatibility, non-irritant having the ability to accelerate the regeneration of epithelial tissue and enhance the restoration of other tissue at the affected site. The positive charge of chitosan gives the polymer an antibacterial effect. In contrast, the positive nature enables the compound to conjugate or bind with various anionic compounds, anti-bodies or aptamers (Lu et al., 2022; Sheikh et al., 2022). Due to various advantages such as biocompatibility, biodegradability, non-antigen, bio-adhesion, antibacterial activity and haemostasis properties, chitosan was selected as the polymer of choice for the preparation of topical hybrid nanocarrier (Lu et al., 2023; Sun et al., 2022).

In the present study, we focused on preparing GA-loaded hybrid nanoparticles by ionic interaction between lecithin and chitosan, where lecithin will provide greater penetration across the stratum corneum along with preserving the trans-epidermal moisture due to the lipidic nature which is very important in the case of psoriasis treatment (Pramual et al., 2017; Pukale et al., 2020). On the other hand, the bio-degradable, non-toxic polymer chitosan will give stability to the product and better retention ability at the site due to adhesiveness and most importantly will provide anti-inflammatory action due to its positive nature. The ideal anti-psoriatic formulation should remain at the specific site for a long time, protect the inflammation, provide a moist environment, and also release the drug-loaded nanoparticles locally in a sustained manner. For fulfilling all this purpose drug loaded nanoparticles were loaded into gel (Fereig et al., 2021a; Sharma et al., 2020). All the results obtained from the experiments indicated that the permeability of GA was increased due to the use of the designed nanocarrier and the efficacy shown by the formulation in the *in vivo* study suggests that the preparation could be a future choice to control psoriasis without any side effects.

2. Experimental

2.1. Materials

Lecithin was purchased from Sigma Aldrich; low molecular weight chitosan was obtained from Loba chemie. Acetic acid, tween, and rhodamine were obtained from S. D fine chemicals, Hi-media and Loba Chemie, India respectively. Other solvents and chemicals used were of analytical grade.

2.2. Preparation of GA-loaded lipid-polymer hybrid nanoparticles

GA-loaded lipid-polymer hybrid nanoparticle (GALPHN) was prepared by a modified ionic-gelation method followed by self-assembly to form a lipidic coating over the drug-loaded chitosan core which has been mentioned below.

2.2.1. Formation of GA-loaded chitosan nanoparticle

Chitosan nanoparticle was prepared by ionic-gelation method. Briefly, 0.1% w/v chitosan solution (cationic solution) was incorporated in acetic acid (5%v/v) solution and the pH was balanced to 4–5.5. Sodium tripolyphosphate (Na-TPP), which is an anionic solution was used as a crosslinking agent in which GA was dissolved. The execution of ionic bonding was achieved through ionic interaction between Na-TPP and chitosan. To develop nanoparticles of chitosan, GA-loaded Na-TPP (0.1% w/v) was incorporated drop by drop into the solution of chitosan solution at 37 °C under constant stirring. The solution was kept on stirring for 2 h, centrifuged for 15 min at 10,000 rpm and re-dispersed to eliminate any free chitosan or Na-TPP (Kongala and Mamidala, 2023).

2.2.2. Development of lecithin-chitosan hybrid nanoparticles (GALPHN)

Lecithin-chitosan hybrid nanoparticles were made by the self-assembly method. The optimum quantity of soy-lecithin was added to 4% hydroalcoholic solution and heated up to 65–70 °C until it gets dissolved (Pramual et al., 2017). The solution of chitosan nanoparticle was further added dropwise to the lecithin solution keeping the solution on mild heating to avoid the formation of lipid vesicles. The solution was kept on continuously stirring at 1000 rpm for the formation of uniform-sized nanoparticles (Baghdan et al., 2018).

2.3. Box-Behnken design optimization

In recent days, the use of optimization methods to optimize the

Table 1
Variables used to optimize the formulation using Box Behnken design.

Independent variables	Low level (−)	Mid-level (0)	High level (+)
A = Lipid concentration (%)	10	20	30
B= Concentration of TPP (%)	23	33	43
C= Sonication time (sec)	30	60	90
Dependent variables			
Z1 = Particle size (%)	Low		
Z2 = PDI	Low		
Z3 = Entrapment efficiency (%)	high		

Table 2
Response obtained from Box Behnken design of optimization for lipid-polymer hybrid nanoparticles.

Code	Independent variables			Dependent variables		
	A	C	B	Z1	Z2	Z3
F1	−	−	0	105.8	0.2295	79.5
F2	−	+	0	33.34	0.307	56.25
F3	+	+	0	247.47	0.236	95.5
F4	−	0	−	64.09	0.079	59.125
F5	+	0	−	278.21	0.1508	91.875
F6	0	0	0	170	0.18	91
F7	0	−	+	218.33	0.5103	88.375
F8	−	0	+	75.5	0.386	67.125
F9	0	−	−	207.38	0.1338	90.375
F10	**0**	**0**	**0**	**170**	**0.18**	**91**
F11	0	+	−	134.93	0.1398	68.625
F12	0	0	0	170	0.18	91
F13	0	0	0	170	0.18	91
F14	+	−	0	319.92	0.452	99.99
F15	+	0	+	289.17	0.4573	94.875
F16	0	+	+	145.88	0.37	81.625
F17	0	0	0	170	0.18	91

formulation employing design of experiment (DOE) has gained enormous attention (Bowden et al., 2019). Various approaches of DOE are available for optimization among which Box-Behnken design (BBD) was chosen as it needs less number of runs and hence can rapidly deliver good results (Imam et al., 2014; Jahangir et al., 2017). The dependent and independent variables selected for the optimization were shown in Table 1 and the experiment-based constituents of the dependent variables are mentioned in Table 2. The selection of the exact ratio for the preparation of the GALPHN was done to obtain a higher entrapment efficiency value and minimum particle size and poly dispersity index (PDI) (Kapoor et al., 2019; Moolakkadath et al., 2018).

2.4. Particle size

The diluted samples were vortexed to determine the size of a particle using Zeta sizer (Malvern instrument UK). A particle size of <500 nm is acceptable for topical use and a PDI of <0.3 can be considered as acceptable homogeneous.

2.5. Entrapment efficiency

The entrapment efficiency (%) of the prepared GALPHN formulation was evaluated by the indirect method. The supernatant of the freshly prepared formulation was taken and diluted to measure the absorbance at 215 nm using a UV spectrophotometer (Shimadzu) for determining the concentration of the free drug. By using the below-mentioned formula entrapment percentage of the drug, and the amount of loaded drug were determined (Fereig et al., 2021b).

$$Entrapment\ efficiency = \frac{Weight\ of\ total\ drug - Weight\ offree\ drug}{Weight\ of\ total\ drug} * 100$$

$$Drug\ loading\ capacity = \frac{Amount\ of\ total\ entrapped\ drug}{Total\ nanoparticle} * 100$$

2.6. Transmission electron microscopy

The morphology of GALPHN was assessed using a transmission electron microscope (TEM) wherein a drop of the sonicated preparation was put on a copper grid and left for drying for 10 min and rinsed 2–3 times with water. 10 μL phosphor-tungstic acid was used to stain the sample. The images were obtained by using the soft imaging viewer software of TEM (200 kV, TECNAI G2, HR-TEM FEI).

2.7. Fourier-transform infrared spectroscopy (FT-IR)

To check the purity of the drug and to observe the changes that occurred after encapsulation of the drug into the nanoparticle, FT-IR of GA and GAPLHN were performed by using a FT-IR spectrophotometer in a range of 4000–400 cm^{-1}. Pellets of potassium bromide were prepared and analysed for each sample in the above-mentioned region.

2.8. Thermal analysis

Thermal analysis of the lyophilized GALPHN formulation was done by using differential scanning calorimetry (DSC) instrument (Pyris 6, DSC, PerkinElmer). About 2–3 mg of sample was packed hermetically in a small aluminum pan and DSC thermogram was recorded over a range of 40–400 °C at a temperature increasing rate of 10 °C/min.

2.9. Preparation of GALPHN-loaded gel

For better management of psoriasis, the formulation has to be retained over the affected area, which will enhance the drug action and provide moisture to the skin. Therefore, GALPHN-loaded gel was developed. Carbopol 934 was sifted from sieve no. 60 and added to the solution of GALPHN under continuous stirring. The solution was neutralized with triethanolamine to develop a gel of desired consistency (Ahad et al., 2014, 2017).

2.10. Evaluation of GALPHN-loaded gel

2.10.1. Homogeneity and pH

Homogeneity of the prepared GALPHN-loaded gel was assessed by visual observation and a digital pH meter (Labman) was used to evaluate the pH of the same in triplicate.

2.10.2. Spreadability

Slip and drag properties were employed to evaluate the spreadability of prepared the gel. A transformed apparatus was used which is consist of a glass-slide having a lower edge fixed while the upper structure was supported by a balance having a hook. Weight was applied to the upper plate after placing 1 g m of sample in between the slides. Spread diameter change due to the spreading of the gel by applying weight on the upper plate was noted (Dantas et al., 2016). The below-mentioned formula helped in determining the spreadability.

$$S = \frac{W * L}{t}$$

Where, 'S' is the spreadability (g/sec), 'L' is fixed length displaced by the glass slide 'W' is the weight on the plate (gm), and 't' is the time (sec) taken to separate the slides.

2.10.3. Texture analysis

Various textural parameters like consistency, cohesiveness, firmness, etc., were determined by performing texture analysis of the prepared GALPHN gel. About 30 g m of gel was placed under the probe of the

texture analyser by placing it into a 100 ml beaker. To circumvent early triggering, the surface of the gel was kept as flat as possible and the sample was placed carefully to avoid air entrapment (Hägerström and Edsman, 2003). The texture was analysed by using a texture analyser (Stable micro system, UK) in compression mode.

2.11. Drug release study

The in-vitro drug release experiment was carried out in a Franz diffusion cell with a dialysis membrane inserted between the acceptor and donor compartments. The membrane was first cleaned under running water, then treated with 0.3% sodium sulphide solution for about a minute before being heated in water at 60–70 °C. The membrane was again treated with 0.2% sulfuric acid for acidification. The membrane was again rinsed with hot water of 60–70 °C for two to 3 min and then left overnight in a PBS solution of pH 5.5. An activated dialysis membrane was then placed in between the donor and acceptor compartment of the Franz diffusion cell. PBS: Methanol solution was added to the acceptor compartment while the donor compartment was loaded with GALPHN gel equivalent to 2 mg drug while maintaining the whole system at 600 rpm and 32 ± 0.5 °C temperature. 1 ml of sample was replaced with fresh Methanol: PBS solution at regular time intervals of 0–24 h to maintain the sink condition (Gupta et al., 2022; Qadir et al., 2020). The same procedure was also carried out for simple GA-loaded gel as a control. To analyse the withdrawn samples UV-spectrophotometer was used at a specific wavelength of 215 nm.

2.12. Skin permeation study

To conduct the permeation study, the skin of mice was excised and placed on Franz diffusion cell with 1 cm^2 diffusion area for 6 h. A portion of skin was placed in between the acceptor and donor compartment after the removal of hair from the whole epidermis side of the skin was facing the PBS: Methanol at the acceptor compartment (Prasad et al., 2014). The donor compartment was filled with GALPHN gel equivalent to 6 mg of GA. The system was maintained at a temperature 32 ± 0.5 °C while the acceptor compartment was stirred continuously. 1 ml sample was withdrawn at regular time intervals and immediately replaced with an equal volume of fresh buffer solution (Singh et al., 2013). The filtered and diluted samples were then analysed by UV-spectrophotometer at 215 nm.

2.13. Skin permeation study by confocal laser scanning microscopy (CLSM)

For the *ex-vivo* permeation study, Rhodamine B-loaded lipid-polymer hybrid nanoparticles were prepared. Freshly prepared nanoparticles were then homogeneously applied over the hair-free skin of mice without any plaque and placed on diffusion cell separately for 8 h maintained at 32 ± 0.5 °C temperature. The formulated treated skin was washed with water and methanol to remove the spare amount of rhodamine. Slides were then prepared from the skin samples and analysed under a confocal laser scanning microscope to determine in-depth permeation (Ali et al., 2019; Qadir et al., 2020).

2.14. Skin permeation enhancement study

This interaction study was done by performing differential scanning calorimetry (DSC) and FT-IR of GALPHN gel-treated skin and comparing it with untreated skin as a control. Excised mice skin was placed on Franz diffusion cell containing PBS in the receptor compartment and treated with GALPHN gel for 8 h and another skin was mounted but kept untreated to use as a control. After 8 h both the skin were collected and cleaned by using distilled water. After proper drying skin samples were cut into pieces to perform DSC and FT-IR (Gupta et al., 2022; Qadir et al., 2020).

2.15. Hen's egg test-chorioallantoic membrane (HET-CAM) assay

Fertilized leghorn chick eggs were obtained from a poultry farm, Gurgaon, Haryana, India. Before incubating the eggs were checked visually for any breakage of the outer shell. Unaffected eggs were incubated under controlled conditions of 37 ± 0.2 °C temperature and 60–70% humidity, until the experiment. On the tenth day after aseptically removing a portion of the eggshell, the test samples were applied carefully over the CAM surface. Then they were allowed to come into contact properly for 5 min. The tested groups included 0.9% NaCl solution as a negative control, 0.1 N sodium hydroxide as a positive control, GALPHN gel, and GA suspension for irritancy comparison. The irritation potential of each sample was assessed by tracking three end points for 5 min each: coagulation, lysis, and haemorrhage. Results were assessed by comparing the Irritation Score (IrS) as 0.0–0.9 as Non-irritant, 1.0–4.9 as slightly irritant, 5.0–8.9 as moderately irritant, and 9.0–21.0 as severely irritant. The changes were continuously observed over 10 min and the point at which irritation occurs was noted. After completion of the observation images were taken and IS was calculated by using the following formula as mentioned by Weimer and associates ("Het Cam," n. d.).

$$IrS = [(301 - H /300) \times 5] + [(301 - L /300) \times 7] [(301 - C /300) \times 9]$$

Where, "IrS" stands for irritation score, H is the start second of haemorrhage effect, L is the start second of lysis effect, and C is the start second of coagulation effect.

2.16. In vivo animal study

The BALB/c mice were obtained from Jamia Hamdard's Central Animal House Facility (CAHF) in New Delhi, India. The IEAC, Jamia Hamdard, New Delhi, approved (Proposal no. 1980) to conduct the *in vivo* investigations, and their recommendations were followed. The animals were permitted to consume the regular laboratory feed and drink water at will, and they were housed in standard laboratory settings.

2.17. Skin irritation study

To investigate the safety of the produced GALPHN gel against 0.8% v/v formalin, a relative skin irritation experiment was performed on BALB/c mice. Animals were kept in conventional laboratory conditions, and the formulation was applied to the mice's dorsal skin. Visual observation of the application site was used to provide grades [41]. Two groups of animals were given the prepared formulation as well as the formalin solution. To test the irritation, samples were put to the dorsal skin of the mice and visual grading for edema as well as erythema were used. The adjacent untreated skin was used as a control. The Primary Irritation Index (PII) was evaluated using the score of primary irritation (SPI (Ali et al., 2019).

2.18. In-vivo anti-psoriasis study

IMQ induced psoriatic model was used to determine the anti-psoriatic effect of the prepared formulation. Psoriasis-like lesion was induced by applying 12.5 mg of marketed IMQ cream 5% (Imiquad, Glenmark) daily over hair less back of BALB/c mice for 7 days (Sun et al., 2013). Induction of psoriasis was assessed by the development of erythema, and plaques on the IMQ applied area of the skin. For the assessment of anti-psoriatic activity, prepared GALPHN gel was applied over the affected area of the skin. The other groups were treated with the standard marketed formulation of clobetasol propionate and calcipotriol (Pacitrex C). To evaluate the condition of the affected and treated area of the skin, Psoriasis Area and Severity Index (PASI) score was used (Panonnummal et al., 2017; Parmar et al., 2017). For the calculation of PASI score, the presence of erythema, thickness and scaling in all the

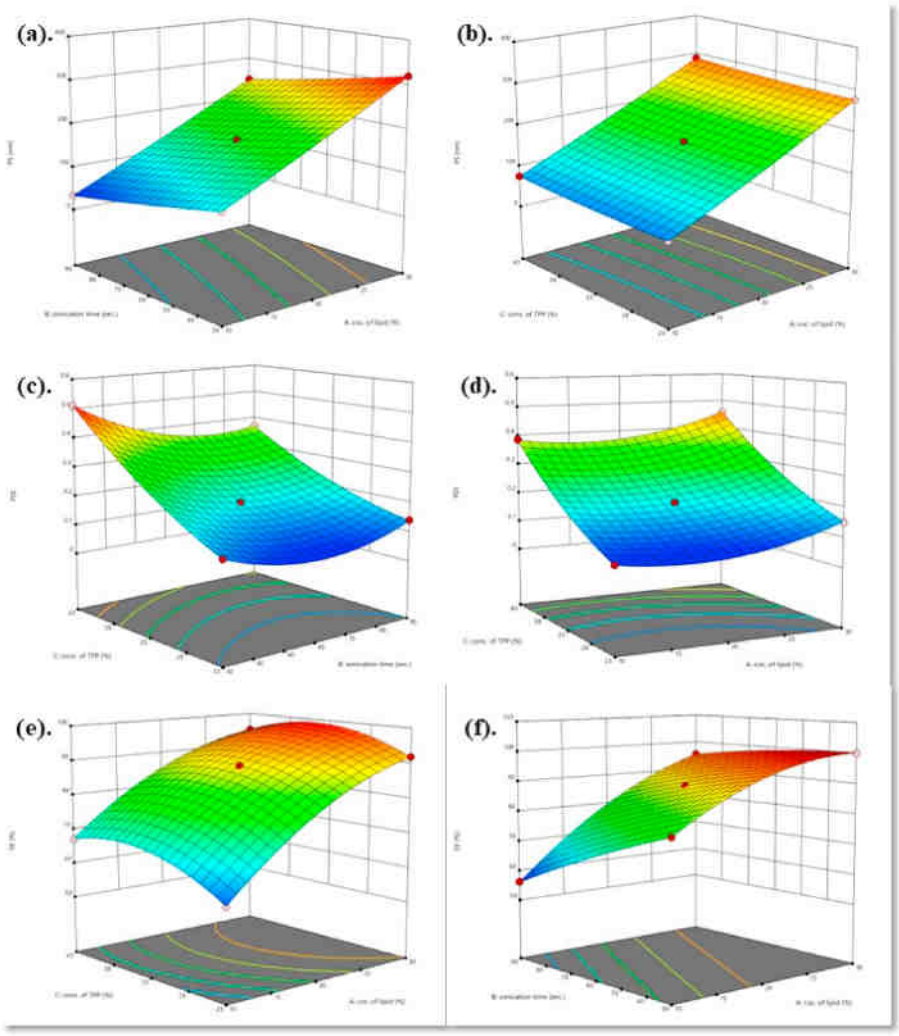

Fig. 1. Effect of independent variables on the particle size [(a)–(b)].; PDI [(c)–(d)]; entrapment efficiency [(e)–(f)].

groups of animals were graded on a scale of 0–4 based on visual observation, according to the method mentioned by Qadir and associates (Qadir et al., 2020).

2.19. Morphological changes in spleen

After sacrificing, spleen was collected from the mice of each group and examined for changes in size of the spleen in different groups, visually and by taking pictures. All the spleens from each group were weighed and compared. The weight of the spleen to the body weight ratio was used to assess the splenomegaly (Sharma et al., 2020).

2.20. Histopathological study

The histopathological study of the affected and treated skin was carried out after the end of the treatment to evaluate the histopathological changes that ensued in different treatment groups during the psoriatic model development (Sharma et al., 2020). The skin samples from different treatment groups were collected after sacrificing the animals and stored in 10% formalin solution. The skin samples were then fixed with paraffin wax (60–62 °C) and cut into sections of 5 μm in thickness using a microtome (Imam et al., 2017). Hematoxylin and eosin (H&E) dye were used to stain the skin sections for better visibility and were observed under a light microscope (Olympus BX 50).

3. Results and discussion

3.1. Optimization

Optimization of GALPHNs was done by using Box Behnken Design (BBD) which gave 17 runs (**Table 2**) with five replicate runs. The quadratic model was found to have the best fit for all of the observed responses. The three-dimensional plots also demonstrated a comparative influence of independent variables on all three dependent variables as represented in Fig. 1. The effect of each factor on their dependent responses as well as the effect of two factors on any response can be evaluated by using these three-dimensional plots.

3.2. Effect of independent variable on particle size (PS)

The 3D plot (Fig. 1) revealed the distinct and combined effects of various independent variables on the size of particles. (a), (b)). Any change in lipid concentration will impact the size of particles [46]. The size of the nanoparticles decreased as the ratio of the concentration of lipid decreased, whereas the size of the nanoparticles increased as the lipid concentration increased. This could be due to the fact that at higher concentrations of lipid and improper heating, the lipid may self-assemble or trigger coalescence, which may also cause particle size increase and formation of improper particles [47]. Particle size decreased as sonication time increased. Very short sonication times resulted in the

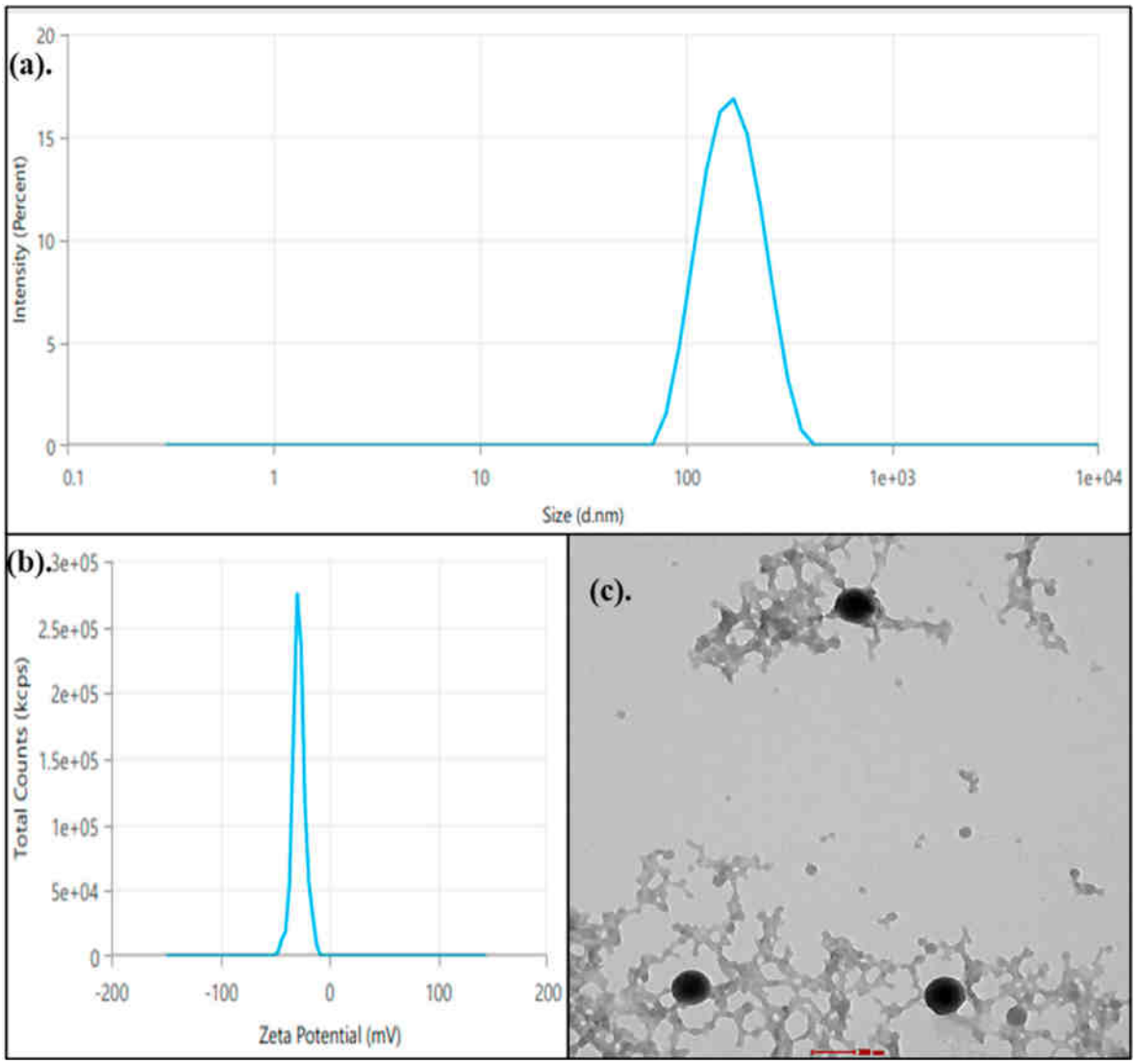

Fig. 2. Particle size and zeta potential of GALPHN formulation [(a), b]; TEM image of prepared lipid-polymer hybrid nanoparticle (c).

formation of large-size nanoparticles, whereas very long sonication times may result in the disintegration of nanoparticles, the release of drug, and the formation of larger particles [48]. As a result, an intermediate sonication period would be appropriate for obtaining nanoparticles in the desired size range. The particle size of all 17 formulations spans from 33.34 to 319.92 nm, with the majority of them being primarily suitable for topical drug administration.

3.3. Effect of independent variables on poly dispersity index (PDI)

Polydispersity index (PDI) is a measure of uniformity in the distribution of preparation which is observed within the acceptable range. A lower value of PDI for any Nano-formulation is desired as it suggests the homogeneous nature of the formulation, while the higher value indicates the heterogeneity of the formulation (Danaei et al., 2018). A wide range of PDI was observed from the results which might be because of the involvement of various independent modalities used for optimization. The 3D plot (Fig. 1. (d), (e)) demonstrated the individual and combined potential of different independent variables over PDI. An increase and decrease in the concentration of lipid and TPP lead to an increase and decrease in the PDI respectively. Less effect of sonication time on PDI was observed. Although extremely higher and lower sonication time was observed to be increasing the PDI, which might be due to the non-uniformity caused by the formation of lower and higher size particles respectively.

3.4. Effect of independent variable on entrapment efficiency (EE)

Entirely, the three independent variables were observed to be affecting the entrapment efficiency of the formulation. A wide range of 55.25–99.99 for entrapment was observed **(Table 2).** Single or combined effects of various independent variables over the entrapment efficiency were observed from the 3-D plot, shown in Fig. 1. (e), (f). The entrapment efficiency of GA was shown to rise with increasing lipid concentration, which is likely due to a rise in nanoparticle size and greater room to entrap the drug. Sonication time was observed to be having a slight effect on entrapment but drug entrapment was decreased with an increase in the sonication time. The drop or spike in EE could be attributed to particle size reduction and enhancement as sonication time is increased or decreased. A higher concentration of crosslinking agent will give the nanoparticles more space to entrap the drug, which could be the reason behind the higher entrapment efficiency observed on the increase in the concentration of TPP.

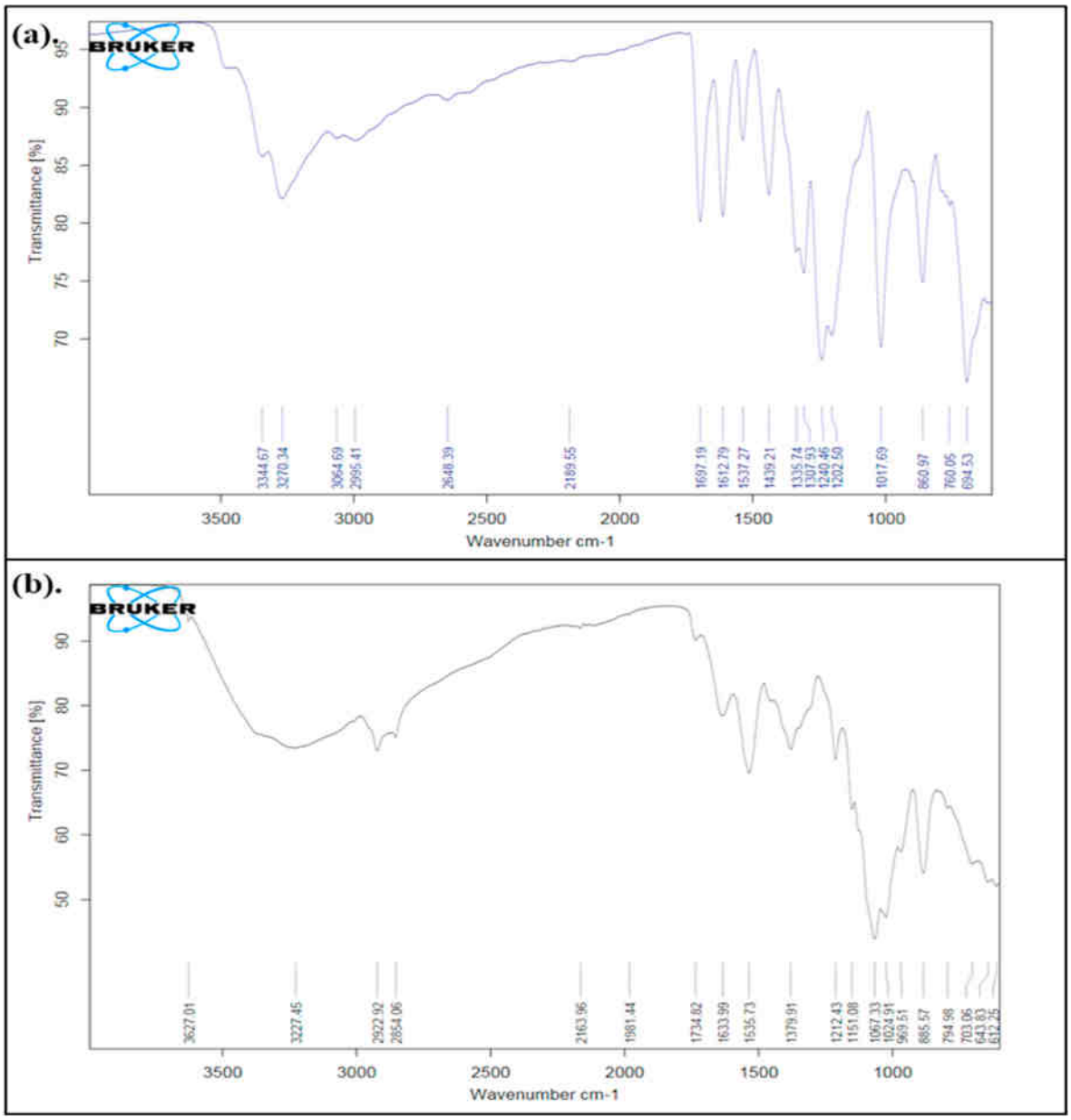

Fig. 3. FT-IR spectra of Gallic acid (a); GA loaded nanoparticles (b).

3.5. Point prediction

After fitting all 17 formulation responses to several kinetic models using software, the quadratic model emerged as the most appropriate fit model for the constructed formulations. As all the independent variables are individually or collectively had a significant effect on the dependent variables, so the quadratic model is the most optimum model for the formulation. It was observed that the experimental values obtained and the experimental values predicted by the software were close and proportional to one another. The optimized GALPHN was designated based on the desired dependent variables. The decision was made to obtain the smallest particle size and PDI while keeping the entrapment efficiency as high as feasible by using the software's point prediction algorithm. Based on the response and desired values of independent variables, the formulation composition with 20% lipid, 33% TPP and 60 s of sonication for the preparation was observed to be consummating the needs of an optimized preparation based upon the combined expectation of all three independent variables. The optimized preparation showed an entrapment efficiency of 89 ± 0.143%, with a particle size of 170.5 ± 0.087 nm and with a PDI of 0.19 ± 0.0015 and zeta potential of −27.97 mV (Fig. 2. (a) And b). 63.57 ± 0.001% drug loading was observed for the optimized formulation. By using the BBD approach of optimization, the optimized combination of factors was selected to prepare the optimized GALPHN, which was then converted to gel according to the requirement and carried forward for further studies.

3.6. Transmission electron microscopy

Transmission electron micrograph of GALPHN formulation has shown well-defined spherical structured nanoparticles. The micrograph demonstrated uniform distribution with distinct boundaries as depicted in Fig. 2. (c).

3.7. Fourier transform infrared spectroscopy (FT-IR)

The FT-IR result of GA showed different characteristic absorption bands owing to the presence of distinct functional groups demonstrated in Fig. 3. (a). The presence of C═O stretching suggested the presence of

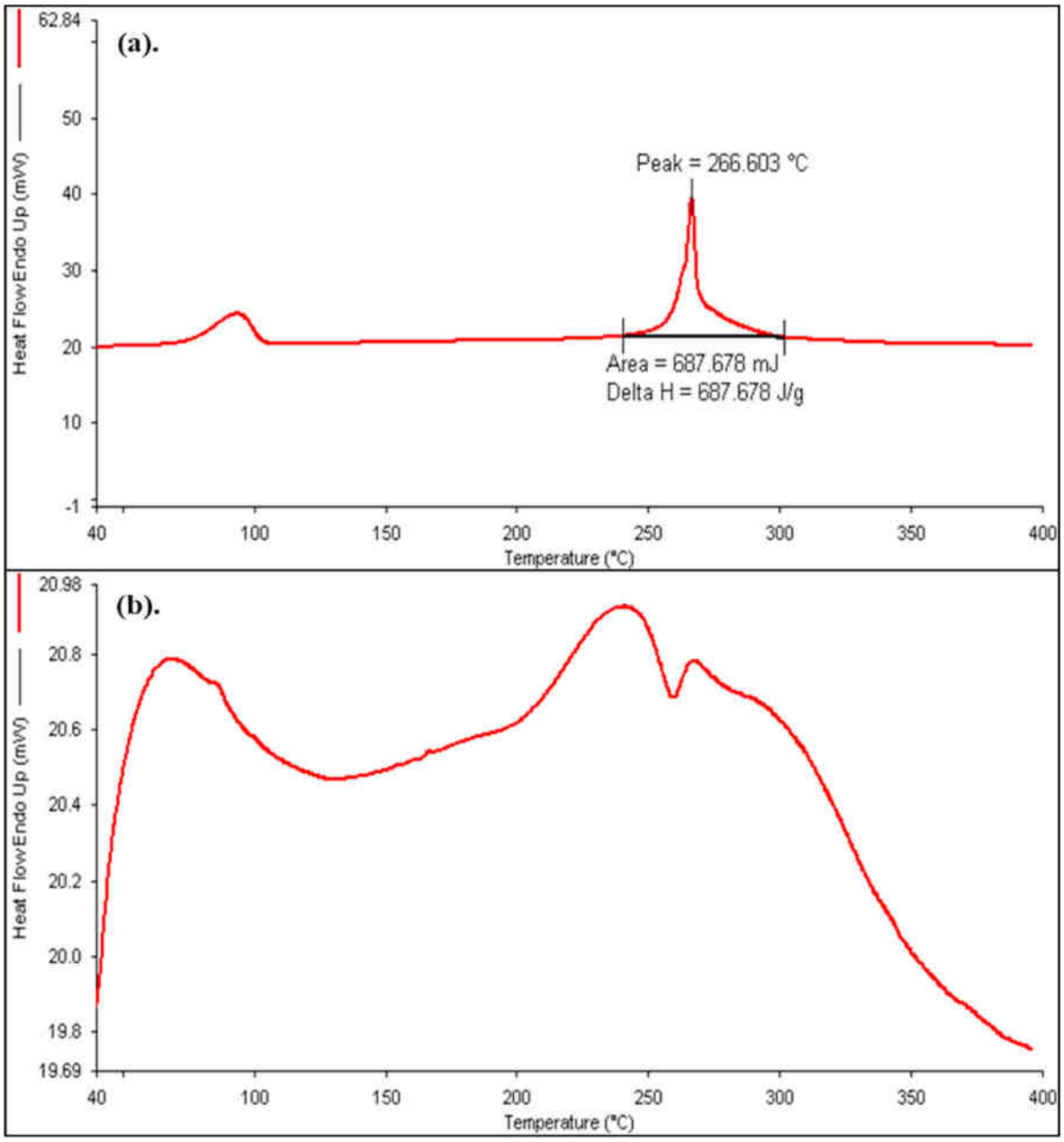

Fig. 4. DSC thermogram of Gallic acid (a); GA loaded nanoparticles (b).

Table 3
Physical evaluation of GALPHN gel.

Physical evaluation of GALPHN gel			
Homogeneity	Good	Cohesiveness (gm)	−150.95
pH	5–6	Consistency (gm.sec)	217.68
Spreadability (g.cm/sec)	15.766 ± 0.404	Work of cohesion (gm. sec)	−261.56
Washability	Easily washable	Firmness (gm)	187.29

a peak at 1697.19 cm^{-1}. The bands at 3500, 3344.67 and 3270.34 cm^{-1} suggest the presence of O–H stretching connected with the benzene group while the absorption band at 3064.69 cm^{-1} corresponds to O–H of the carboxyl group. The presence of an aromatic ring caused C–H stretching, resulting in a band at 2995.41 cm^{-1}. The bands in the 1350 - 1600 cm^{-1} and 700 - 800 cm^{-1} ranges are accounted for the aromatic ring's C═C stretching and C–H bending, respectively. The observation from the FT-IR data of the pure drug is closely similar with the data reported by Hirun et al. (2012) which suggests the authenticity of the procured drug. The formulation's FT-IR spectra (Fig. 3. (b)) revealed an absorption band at 1633.99 attributed to C═O stretching. The presence of a carboxyl group (C═O) showed a peak at 1734.82 cm^{-1} indicating that chitosan has been coated with lecithin. The sharp peak for GA at 1697 cm^{-1} was displaced to a broad and petite peak at 1734 cm^{-1}, showing drug entrapment in the nanoparticle.

3.8. Thermal analysis

The difference in thermal behaviour was observed for GA and GALPHN (Fig. 4) which might indicate the characteristic nature and drug entrapment. A sharp endothermic peak of GA at 266.603 °C authenticates the drug as per the melting point and DSC data also mentioned by Celep and associates (Sagdicoglu Celep et al., 2022). The

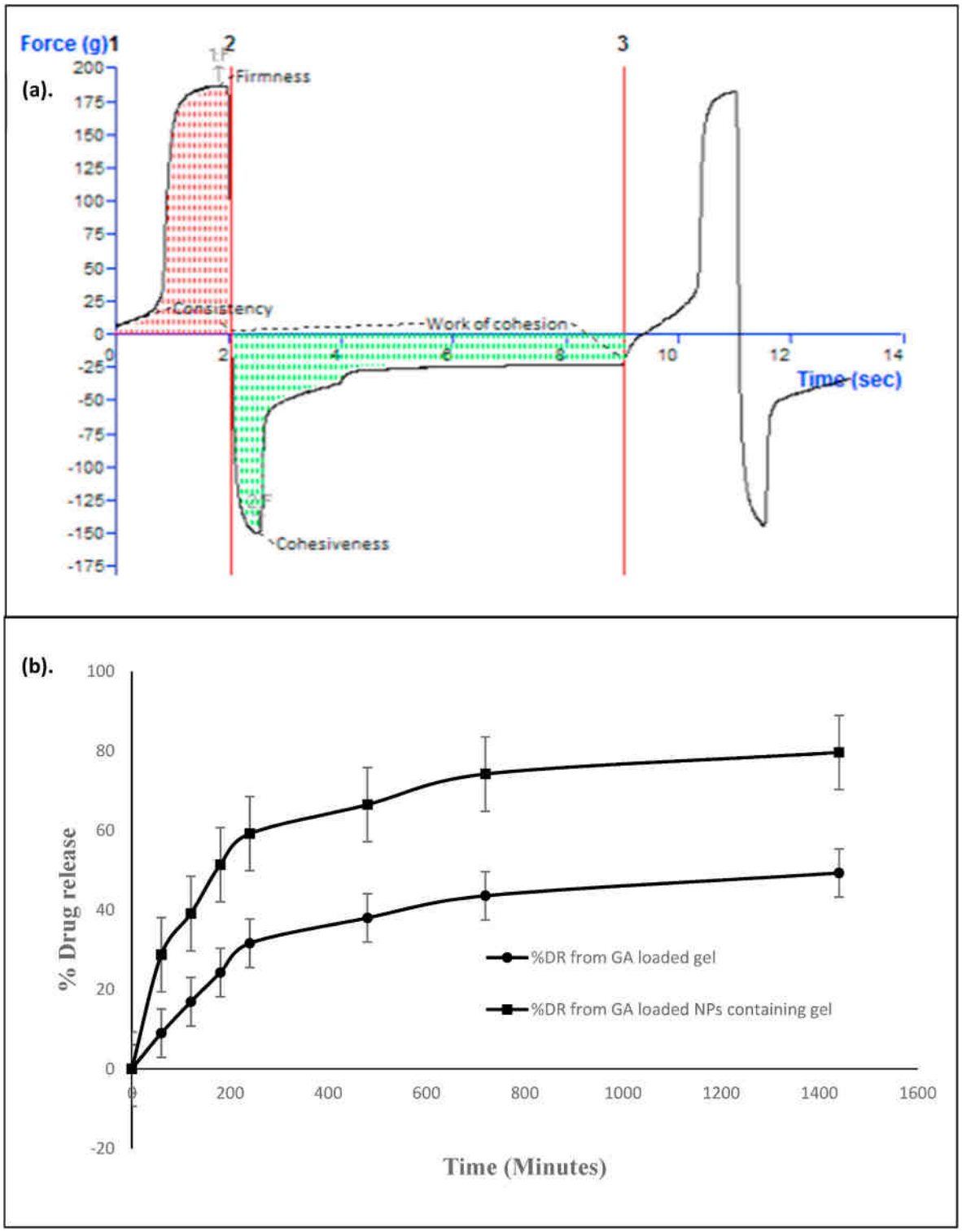

Fig. 5. Assessment texture analysis of the GALPHN gel denoting consistency, firmness, cohesiveness, and work of cohesion (a); Comparative *in vitro* release profile of GA loaded nanoparticles containing gel and GALPHN gel (b).

absence of any sharp peak in the thermogram of GALPHN suggests the encapsulation of the drug. The presence of an unentrapped drug on the surface caused a sharp peak at 265 °C, while the first two bumps in the thermograph were caused by the presence of soy lecithin outside of the nanoparticle, as mentioned by Yusuf and colleagues, implying lecithin coating (Sharma et al., 2014).

3.9. Evaluation of GALPHN gel

Various physical parameters of the prepared GALPHN gel were assessed as mentioned in Table 3. A smooth, pleasant and homogeneous appearance was observed of the prepared gel, with an absence of any grittiness. The pH of the gel was observed to be 5–6, which can be considered safe for topical use without irritating the skin. Spreadability is one of the key parameters of gel for uniform distribution of the drug

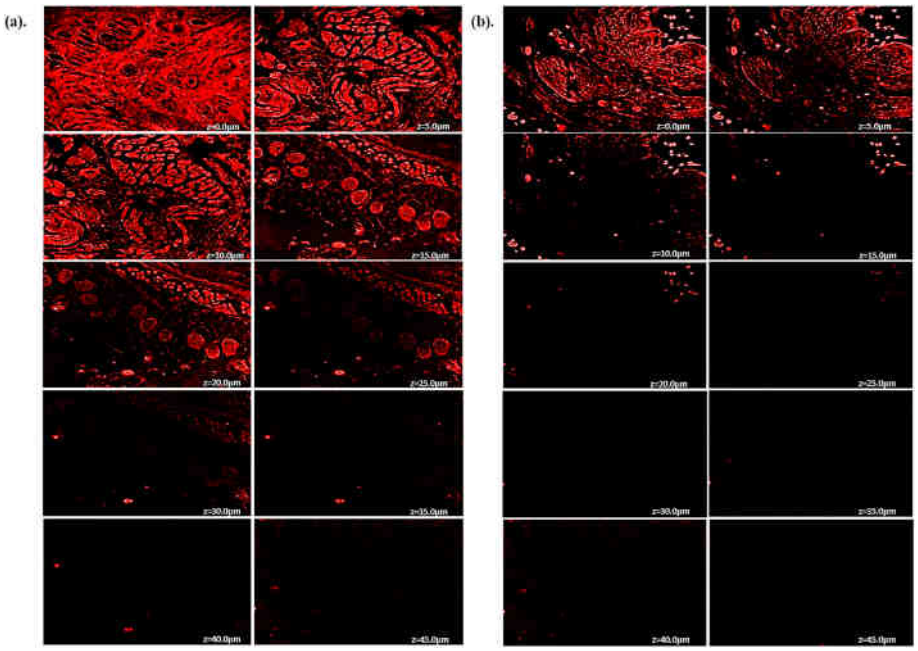

Fig. 6. Confocal micrographic images of mice skin treated with GALPHN gel (a), and hydroalcoholic solution of Rhodamin B (b).

over the skin and was found to be 15.766 ± 0.404 g cm/sec which can be suggested as good as mentioned by Qadir et al. (2020).

3.10. Texture analysis

The texture of the prepared GALPHN gel was analysed and different parameters such as cohesiveness, firmness, consistency, and index of viscosity was evaluated. The prepared formulation of GALPHN-loaded 1% Carbopol gel has shown cohesiveness, firmness, consistency, and index of viscosity of −150.92, 217, 187, and −267.57, respectively as mentioned in Table 3. The report generated by the texture analyser is shown in Fig. 5. (a).

3.11. Drug release study

Comparative percentage drug release of GA from GALPHN gel and GA loaded gel were studied for 24 h and were found to be 79 ± 0.1% and 49 ± 4.47%, respectively after 24 h (Fig. 5. (b)). Minimum drug release from the GA-loaded gel indicates low permeability of the drug (BCS Class- III). The higher release rate of the drug in the case of GALPHN gel could be due to the increase in permeability of the drug after encapsulation into the nanoparticle. The GALPHN gel has shown a biphasic manner of drug release. In the first 5 h s, it has shown a rapid release which may be due to the accessibility of the free drug in the formulation. The initial rapid release was surveyed by a slow release of the drug which might be caused by the entrapment of the drug or due to the hindrance in drug diffusion caused by the higher viscosity of the gel (Siepmann and Peppas, 2012). According to the observations, formulation showed initial burst release followed by a steady release. The drug release study data was kinetically analysed using various mathematical models. The korsmeyer-peppas diffusion mechanism ($R^2 = 0.982$) represented the greatest fit in terms of R^2 value, followed by the Higuchi model ($R^2 = 0.9607$) and the zero-order diffusion model ($R^2 = 0.87$).

3.12. Skin permeation study

Remarkably, a higher yield of flux value i.e. 5.22 μg/cm^2/h was observed in the permeation profile of GALPHN gel across the mice skin, which was observed to be much lesser in GA-loaded gel (control) i.e. 1.8469 μg/cm^2/h. Lipidic nanocarriers like liposomes or in the case of any lipid-coated carriers, the presence of lipids on the outer layer increased the permeability of the drug (Xi et al., 2022). The elevation in the permeation profile can be considered due to the entrapment of the drug into the particles made up of lipid and bio-adhesive polymer and having a size range of nanometres. The lipid and polymer used in the formulation enhances the permeability of GA by the outer lipidic nature and helps to retain the epidermis for a longer time due to the bio-adhesive nature of the polymer along with providing stability to the preparation. The nano-size of the particle made the particle enough capable to penetrate the deeper layers of the skin. According to the permeation profile, the assumption of better permeation and retention of the drug across the skin layers suggests that the prepared formulation could be beneficial for the topical treatment of psoriasis.

3.12.1. Skin permeation study by confocal laser scanning microscopy (CLSM)

The enhanced permeability due to the use of nanoparticles has clearly been observed by the confocal laser scanning microscopy. Rhodamine B-treated skin has shown a limited permeation of dye fluorescence up to approximately 20–25 μm through the skin. On another side Rhodamine B-loaded nanoparticles showed better absorption into the deeper layer of the skin with more prominent penetration of sample up to 40–45 μm (Fig. 6). The noticeably higher fluorescence intensity in the mid-skin region suggested that the preparation was retained in a higher concentration in the lower epidermal environment after traversing the upper epidermis (Qadir et al., 2020). Observation from the CLSM images suggests that the entrapment of GA (BCS class-III) into the nanoparticle elevated the drug penetration into deeper layers of the skin.

3.13. Skin permeation enhancement study

The FT-IR and DSC techniques were utilized to evaluate the penetration of GA from the GALPHN gel formulation into the skin as well as its interaction with the skin. The absorption bands in the FTIR spectra of normal skin (Fig. 7. (a)) are caused by the alkyl group C–H stretching present in both lipids and proteins of the stratum corneum, whereas the absorption bands of 2918.94 and 2853.59 cm-1 are caused by symmetric

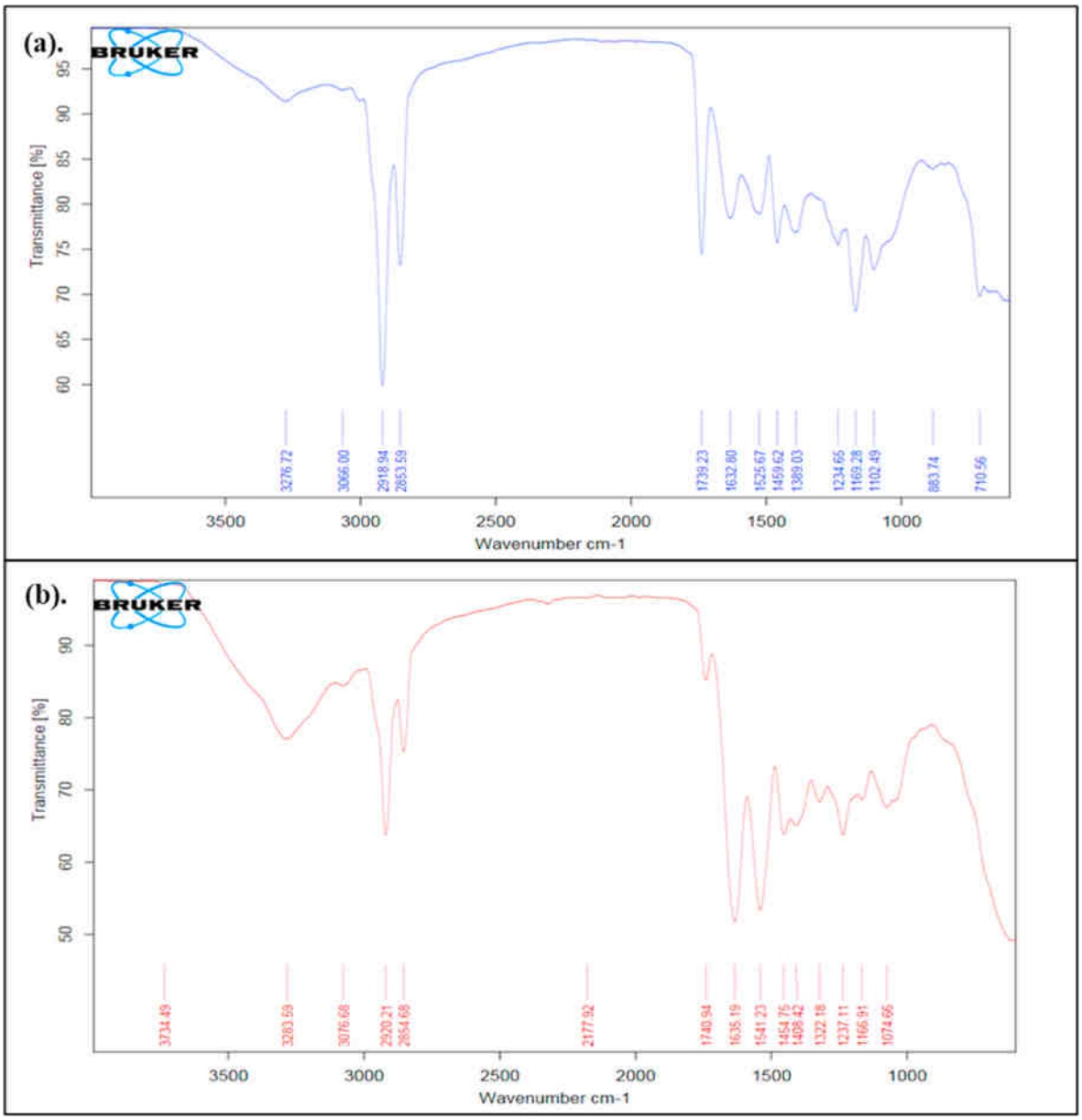

Fig. 7. FT-IR spectra of normal skin (a); GALPHN gel treated skin (b) of mice.

and asymmetric C–H stretching of lipids. The stretching vibrations of the proteins' amide I and amide II created bands at 1632.80 and 1525.67 cm-1. The amide I band is composed of component bands representing different keratin architectures. However, the treated skin revealed displacement of absorption bands in the FTIR spectra at 3734.49, 3283.59, and 3076.68 cm-1 from 3276.72 to 3066 cm-1, indicating formulation interaction with the skin (Fig. 7. (b)). The band at 2854.68 cm-1 represents C–H stretching by the alkane group, the band at 1740.94 cm-1 represents C═O stretching, and the band at 1635.19 cm-1 represents C═C stretching by alkene moieties. The absorption band at 1454.75 cm-1 represents C–H bending (alkane), the band at 1408.42 cm-1 represents O–H bending, and the band at 1074.66 cm-1 represents C═C bending (alkene). The spectra of GA and mouse skin with formulation showed similar characteristic peaks with minimal changes. The discrepancies in peak levels can be explained by the chemical interaction between the skin and GALPHN (Gupta et al., 2022).

DSC thermograms were compared between normal skin and skin treated with the optimized formulation. Normal skin displayed an endothermic peak at 120.858 °C, which might be attributed to skin denaturation of protein, but mice skin exposed to the treatment revealed a peak shift to 129.806 °C (Fig. 8 a, b). The shift in peak position is due to interference in the stratum corneum junction, which is required for better drug penetration (Moolakkadath et al., 2018).

3.14. HET-CAM assay

Irritability and tolerability of the final GA loaded formulation were assessed using HET-CAM test and were compared with the 0.9% w/v normal saline taken as negative control and 0.1 N NaOH taken as positive control groups. Both the negative control and drug-loaded final formulation were observed as non-irritating in comparison with the positive control using IS. For normal saline, the IS was found to be 0.596 ± 0.001 whereas the positive control has shown a score of 16.78 ± 1.01, which is considered a severe irritant. The GA-loaded nanoparticle and GA-loaded suspension have shown a mean irritation score of 0.66 ± 0.0005 and 3.33 ± 0.01 respectively. These observed IS suggested that the entrapment of the drug into the nanoparticle has reduced the irritation potential of the drug from a slightly irritant to a non-irritant level.

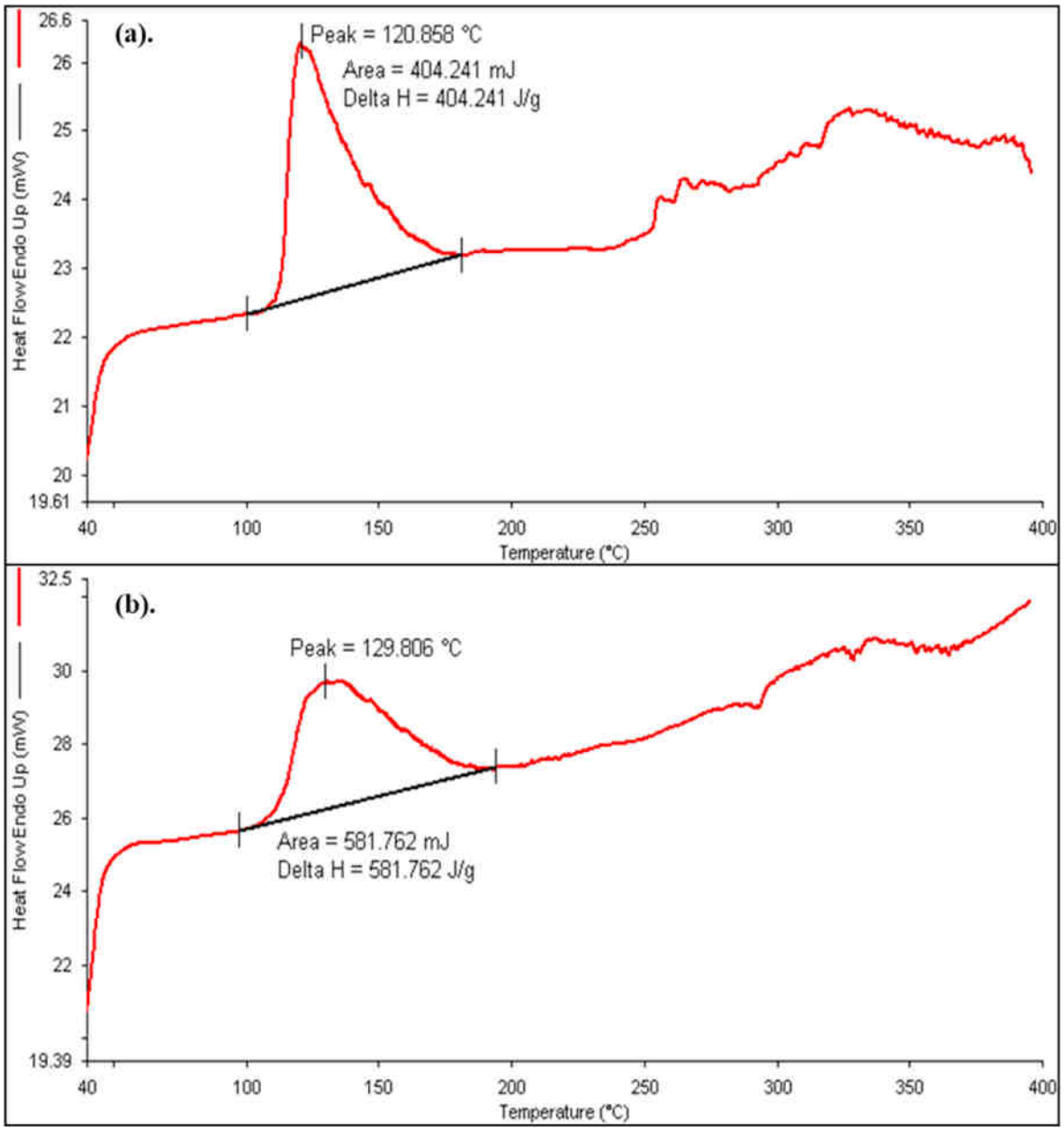

Fig. 8. DSC thermogram of normal skin (a); GALPHN gel treated skin (b) of mice.

This observation showed that the GALPHN gel can be considered as non-toxic, and non-irritating as shown in Fig. 9.

3.15. Skin irritation study

All the scores graded to suggest the extent of erythema and edema for the assessment of irritation induced by standard formalin solution and prepared GALPHN gel in different groups are given in Table 4. The scores of edema attained for negative control, positive control and GALPHN gel were found to be 0.0 ± 0.0, 3.0 ± 0.81, and 0.75 ± 0.95, respectively, while the scores for erythema were found as 0.0 ± 0.0, 2.75 ± 0.95, and 0.75 ± 0.95, respectively. Addition of the scores graded for edema and erythema were used to estimate the primary irritation index (PII) for each group. The calculated PII scores for standard formalin solution as positive control and GALPHN gel were measured to be 5.75 and 0.825, respectively. Any preparation having PII score of 2 or less than that can be measured as non-irritant for skin (Qadir et al., 2020). As the PII score of the prepared GALPHN gel formulation was less than 2, it can be measured as non-irritant to be used topically.

3.16. Evaluation of the anti-psoriatic activity

The psoriasis in animal models was induced by Imiquimod (IMQ), which was characterized by the scaling and thickening of the skin (Qadir et al., 2020). Mice after treatment with IMQ started developing mild thickening, erythema and scaling-like psoriatic symptoms over the dorsal side of skin which began from the 2nd to 4th day after initiation. Visible inflammations were continuously increased up to 7–8 days of the disease induction period. The animals with psoriasis except the positive control group, were subjected to treatment to examine and compare the therapeutic effect of drug and nanopreparation. In the GALPHN-treated group, all the visible signs such as swelling and redness were reduced while no visible changes were observed for the positive control group. As mentioned in Table 5, a score of erythema, scaling, and thickening started reducing from 2nd day of treatment and was recorded as zero after the 5th day, which was confirmed against the negative control

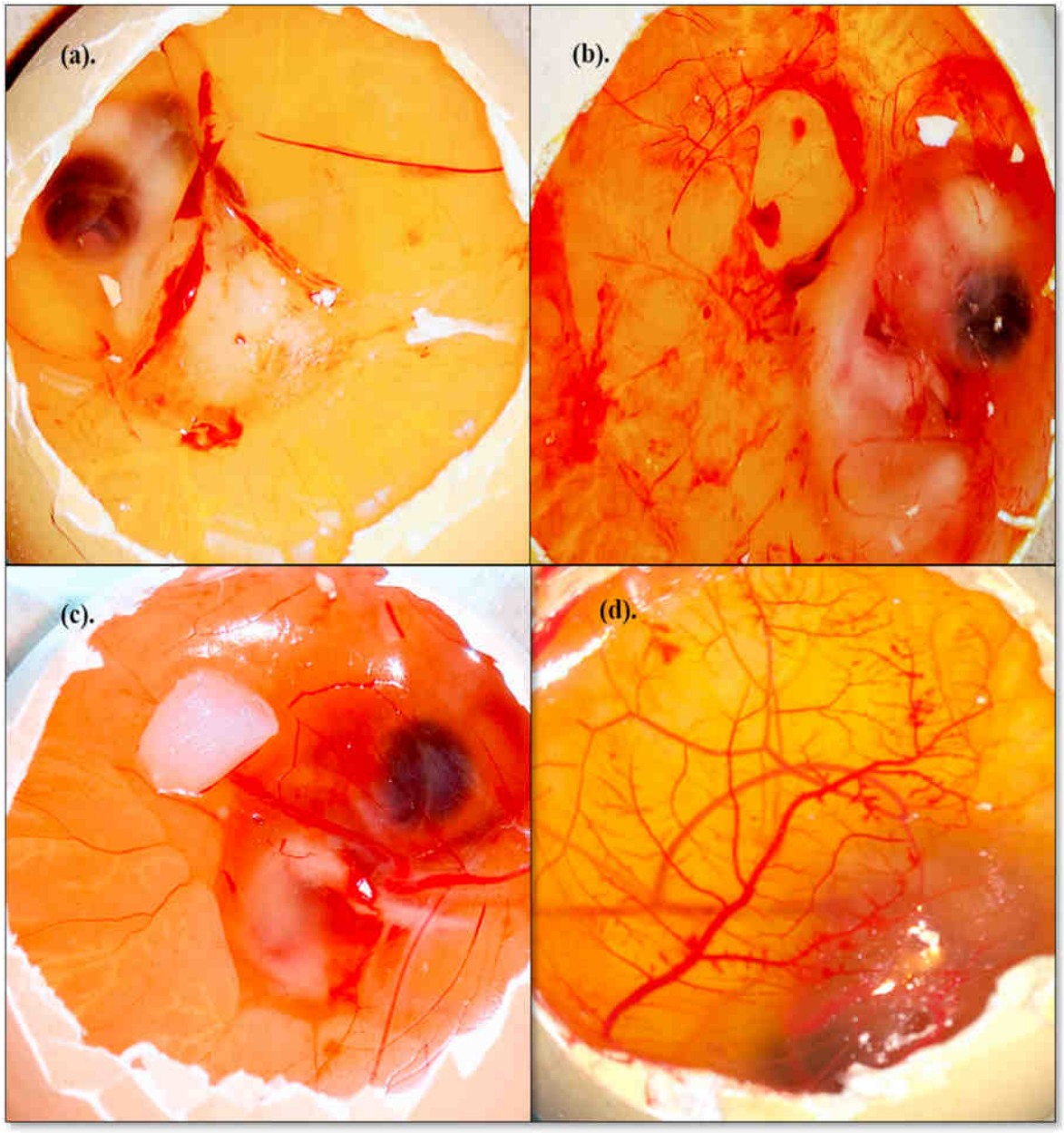

Fig. 9. Images of fertilized egg treated with negative control (a); positive control (b); GALPHN formulation (c); hydroalcoholic solution of GA (d).

Table 4
Mean primary irritation index score obtained from different treated groups.

Group	Control		Formalin (0.8%)		GALPHN gel	
	Erythema	Edema	Erythema	Edema	Erythema	Edema
1	0	0	2	2	0	1
2	0	0	2	3	2	2
3	0	0	4	4	1	0
4	0	0	3	3	0	0
Mean score ±SD	0	0	2.75 ± 0.95	3 ± 0.81	0.75 ± 0.95	0.75 ± 0.95
PII	0		5.75		0.825	

group. Scores were given on a scale of 0–4 (0: none; 1: slight; 2: moderate; 3: marked; 4: very marked). The group treated with standard marketed formulation also showed a reduction in all the functional domains but to a limited extent in comparison with the prepared GALPHN gel as shown in Table 5. On the other hand, the GA-loaded gel has also shown some improvement which was comparatively lesser in both GALPHN gel and the standard marketed formulation. From the observation and score mentioned in Tables5 and it can be concluded that the prepared GALPHN gel was found to be more propitious as compared with the standard marketed formulation and normal GA gel in terms of efficacy. The comparative observation between GALPHN gel and normal GA gel suggested that the better efficacy of GALPHN gel is due to the increased permeation of the drug (BCS Class-III) owing to the encapsulation inside the nanoparticle. The positive control group or toxic group has shown a significantly high score for all seven days.

3.17. Spleen morphology

Enlargement of the spleen is one of the most important signs of immunological disorders. The spleen of all the groups was examined by size and weight at the end of the experiment. A comparative graph of mass of spleen and pictures were shown in Fig. 10. (a). Significantly

Table 5
Calculation of clinical Psoriasis Area and Severity Index (PASI) score based on visible Erythema (ER), Scaling (SC), Thickening (TH).

Day of treatment	Control			IMQ			IMQ + GALPHN gel			IMQ + GA loaded gel			IMQ + Clobetasol		
	ER	SC	TH	ER	SC	TH	ER	SC	TH	ER	SC	TH	ER	SC	TH
0	0	0	0	4	4	4	4	4	4	4	4	4	4	4	4
1	0	0	0	4	4	4	3	2	3	3	3	3	2	3	3
2	0	0	0	4	3	4	2	2	2	3	2	3	2	2	3
3	0	0	0	3	3	4	1	1	2	2	2	2	2	2	3
4	0	0	0	3	3	3	0	1	1	2	2	2	2	1	2
5	0	0	0	2	3	3	0	0	0	1	1	2	1	1	1
6	0	0	0	2	2	3	0	0	0	1	1	1	0	0	1
7	0	0	0	2	2	2	0	0	0	0	1	1	0	0	0
Average PASI	0	0	0	3	3	3.375	1.25	1.25	1.5	2	2	2.25	1.625	1.625	2.125

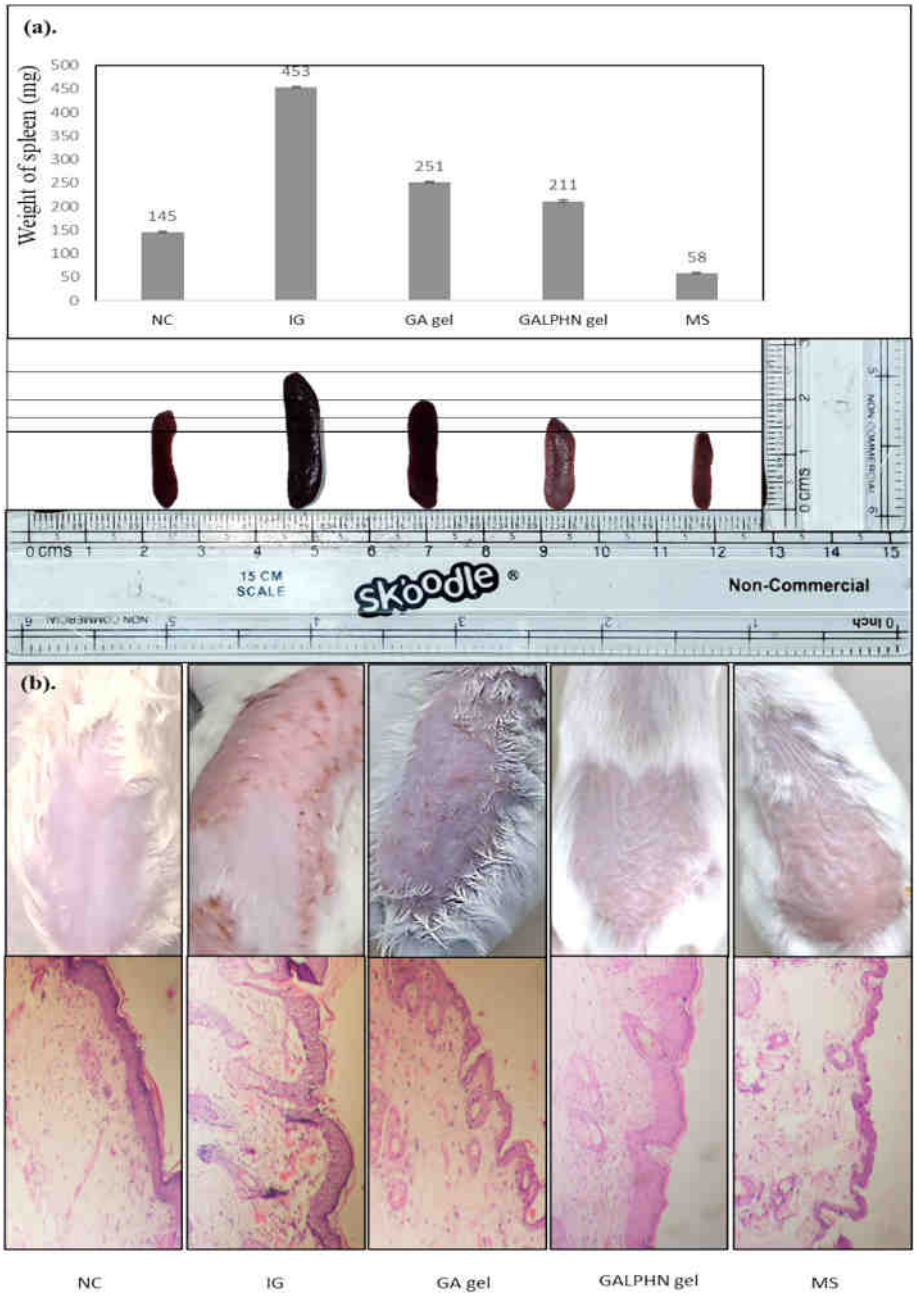

Fig. 10. Weight, size and morphology of spleen (a) and histological characteristics of differently treated groups in comparison with the negative control and induced group (b). [NC- Negative Control; IG- Induced Group (Positive control); GA gel- Gallic Acid loaded gel; GALPHN gel-prepared formulation; MS- Marketed Standard].

enlarged size of spleen was observed in the case of IMQ treated control group as compared to the spleen of the normal control group. The size of the spleen was markedly decreased in GALPHN gel, GA-loaded gel and standard marketed formulation treated groups. Splenomegaly in mice was induced by IMQ by enhancing the number of immune cells. The observed splenomegaly in the case of IMQ treated toxic group is owing to a significant increase in T-cells, dendritic cells and a reduction in macrophages. Marked reduction in the spleen mass and size after topical applications reflect the influence of the formulation over local immunity in psoriatic mice. Because of this, the regulation of local immunity in mice now serves as a strong justification for the systemic influence on the cellular structure of the spleen following topical treatment by GALPHN gel.

3.18. Histopathological study

After 15 days from the initiation of the study, skin samples from all the groups were subjected to histopathological assay to observe any internal alteration. Positive control group and other treated groups were compared with the untreated negative control group (Fig. 10. (b)). Intact epidermis and dermis with viable cells were observed for the untreated negative control group (Fig. 10. (b)). Both the prepared GALPHN gel treated and standard marketed formulation treated group showed intact outer epidermis of skin although the similarity with negative control was more prominent for the prepared GALPHN gel (Fig. 10. (b)). Over-thinning of the outer epidermis and altered lower epidermis was observed for the group treated with the marketed formulation, which might be due to the over-suppression of the immune system. An apparent difference in the epidermis and dermis with an unusual internal orientation of the skin was observed for the positive control group (Fig. 10. (b)). The observation suggests that the prepared GALPHN formulation had better efficacy in restoring the altered cellular behaviour of the epidermis caused by psoriasis without showing any side effects and irritation-inducing properties.

4. Conclusion

In this study, GA was loaded into the lipid-polymer hybrid nanoparticle in view to increase the efficacy of GA against psoriasis by elevating the permeability of the Biopharmaceutical classification system (BCS) Class III drug. The prepared formulation was optimized by using BBD optimization tool. The optimized formulation using the Box-Behnken design showed a size and PDI of 170.5 ± 0.087 nm and 0.19, respectively, suggesting its suitability for topical application. Enhanced penetration as demonstrated by the confocal study and skin permeation study indicated the retention of the maximum drug at the dermal layer of the skin. Better drug permeation and drug release were interpreted from the in-vitro release study. HET-CAM study and other evaluation parameters of the formulation proved the safety index. The *in vivo* study of the GALPHN gel on BALB/c mice demonstrated low skin irritancy and no immunogenic response along with good efficacy of the GALPHN formulation against psoriasis as compared to GA-loaded gel and marketed formulation. Based on the result obtained, the prepared GALPHN gel formulation can be inferred as one of the promising and successful treatments of psoriasis which has the ability to substitute the use of immunomodulators and steroids in the near future. Moreover, the potential therapeutic aspect could be evaluated on cell lines to assess the cellular uptake and their progression.

Credit author statement

Both the authors have been contributed significantly and equally to complete this manuscript.

Declaration of competing interest

The authors declare that they have no known competing financial interests or personal relationships that could have appeared to influence the work reported in this paper.

Data availability

The data that has been used is confidential.

Acknowledgments

The authors would like to thank the ↱Deanship of Scientific Research at Umm Al-Qura University ↱for supporting this work by Grant Code: (22UQU4280449DSR01).

References

Ahad, A., Al-Saleh, A.A., Al-Mohizea, A.M., Al-Jenoobi, F.I., Raish, M., Yassin, A.E.B., Alam, M.A., 2017. Pharmacodynamic study of eprosartan mesylate-loaded transfersomes Carbopol® gel under Dermaroller® on rats with methyl prednisolone acetate-induced hypertension. Biomed. Pharmacother. 89, 177–184. https://doi.org/10.1016/j.biopha.2017.01.164.

Ahad, A., Aqil, M., Ali, A., 2014. Investigation of antihypertensive activity of carbopol valsartan transdermal gel containing 1,8-cineole. Int. J. Biol. Macromol. 64, 144–149. https://doi.org/10.1016/j.ijbiomac.2013.11.018.

Ahamed, J., Jaswanth Gowda, B.H., Almalki, W.H., Gupta, N., Sahebkar, A., Kesharwani, P., 2023. Recent advances in nanoparticle-based approaches for the treatment of brain tumors: opportunities and challenges. Eur. Polym. J. 193, 112111 https://doi.org/10.1016/J.EURPOLYMJ.2023.112111.

Akentieva, N.P., Gizatullin, A.R., Silvestre, O., Savchuk, O., Shkondina, N.I., Prichodchenko, T.P., Mitschenko, D.V., Zhilenkov, A.V., Troshin, P.A., Sanina, N.A., Dremova, N.H., Torbov, V.I., Aldoshin, S.M., Nieder, J.B., 2020. Development of chitosan-hyaluronic acid nanoparticles and study of their physico-chemical properties for targeted delivery of anticancer drugs. IOP Conf. Ser. Mater. Sci. Eng. 848 https://doi.org/10.1088/1757-899X/848/1/012002.

Aldredge, L.M., Higham, R.C., 2018. Manifestations and management of difficult-to-treat psoriasis. J. Dermatol. Nurses. Assoc. 10, 189. https://doi.org/10.1097/JDN.0000000000000418. –197.

Ali, A., Ali, S., Aqil, M., Imam, S.S., Ahad, A., Qadir, A., 2019. Thymoquinone loaded dermal lipid nano particles: Box Behnken design optimization to preclinical psoriasis assessment. J. Drug Deliv. Sci. Technol. 52, 713–721. https://doi.org/10.1016/j.jddst.2019.05.041.

Ashrafizadeh, M., Ahmadi, Z., Mohamadi, N., Zarrabi, A., Abasi, S., Dehghannoudeh, G., Tamaddondoust, R.N., Khanbabaei, H., Mohammadinejad, R., Thakur, V.K., 2020. Chitosan-based advanced materials for docetaxel and paclitaxel delivery: recent advances and future directions in cancer theranostics. Int. J. Biol. Macromol. 145, 282–300. https://doi.org/10.1016/J.IJBIOMAC.2019.12.145.

Ashrafizadeh, M., Delfi, M., Hashemi, F., Zabolian, A., Saleki, H., Bagherian, M., Azami, N., Farahani, M.V., Sharifzadeh, S.O., Hamzehlou, S., Hushmandi, K., Makvandi, P., Zarrabi, A., Hamblin, M.R., Varma, R.S., 2021. Biomedical application of chitosan-based nanoscale delivery systems: potential usefulness in siRNA delivery for cancer therapy. Carbohydr. Polym. 260, 117809 https://doi.org/10.1016/J.CARBPOL.2021.117809.

Ashrafizadeh, M., Hushmandi, K., Mirzaei, S., Bokaie, S., Bigham, A., Makvandi, P., Rabiee, N., Thakur, V.K., Kumar, A.P., Sharifi, E., Varma, R.S., Aref, A.R., Wojnilowicz, M., Zarrabi, A., Karimi-Maleh, H., Voelcker, N.H., Mostafavi, E., Orive, G., 2023. Chitosan-based nanoscale systems for doxorubicin delivery: exploring biomedical application in cancer therapy. Bioeng. Transl. Med. 8, e10325 https://doi.org/10.1002/BTM2.10325.

Aziz, A., Rehman, U., Sheikh, A., Abourehab, M.A.S., Kesharwani, P., 2022. Lipid-based Nanocarrier Mediated CRISPR/Cas9 Delivery for Cancer Therapy. https://doi.org/10.1080/09205063.2022.2121592, 10.1080/09205063.2022.2121592.

Aziz Hazari, S., Kaur, H., Karwasra, R., Abourehab, M.A.S., Ali Khan, A., Kesharwani, P., 2023. An overview of topical lipid-based and polymer-based nanocarriers for treatment of psoriasis. Int. J. Pharm. 638, 122938 https://doi.org/10.1016/J.IJPHARM.2023.122938.

Baghdan, E., Pinnapireddy, S.R., Strehlow, B., Engelhardt, K.H., Schäfer, J., Bakowsky, U., 2018. Lipid coated chitosan-DNA nanoparticles for enhanced gene delivery. Int. J. Pharm. 535, 473–479. https://doi.org/10.1016/J.IJPHARM.2017.11.045.

Bowden, G.D., Pichler, B.J., Maurer, A., 2019. A design of experiments (DoE) approach accelerates the optimization of copper-mediated 18F-fluorination reactions of arylstannanes. Sci. Reports 2019 91 9, 1–10. https://doi.org/10.1038/s41598-019-47846-6.

Cassano, R., Cuconato, M., Calviello, G., Serini, S., Trombino, S., 2021. Recent advances in nanotechnology for the treatment of melanoma. Molecules 26. https://doi.org/10.3390/MOLECULES26040785.

Chen, R., Zhai, Y.Y., Sun, L., Wang, Z., Xia, X., Yao, Q., Kou, L., 2022. Alantolactone-loaded chitosan/hyaluronic acid nanoparticles suppress psoriasis by deactivating

STAT3 pathway and restricting immune cell recruitment. Asian J. Pharm. Sci. 17, 268–283. https://doi.org/10.1016/j.ajps.2022.02.003.
Choubey, S., Varughese, L.R. ache, Kumar, V., Beniwal, V., 2015. Medicinal importance of gallic acid and its ester derivatives: a patent review. Pharm. Pat. Anal. 4, 305–315. https://doi.org/10.4155/ppa.15.14.
Danaei, M., Dehghankhold, M., Ataei, S., Hasanzadeh Davarani, F., Javanmard, R., Dokhani, A., Khorasani, S., Mozafari, M.R., 2018. Impact of particle size and polydispersity index on the clinical applications of lipidic nanocarrier systems. Pharmaceutics 10. https://doi.org/10.3390/PHARMACEUTICS10020057.
Dantas, M.G.B., Reis, S.A.G.B., Damasceno, C.M.D., Rolim, L.A., Rolim-Neto, P.J., Carvalho, F.O., Quintans-Junior, L.J., Da Silva Almeida, J.R.G., 2016. Development and evaluation of stability of a gel formulation containing the monoterpene borneol. Sci. World J. https://doi.org/10.1155/2016/7394685, 2016.
Dongsar, T.T., Dongsar, T.S., Abourehab, M.A.S., Gupta, N., Kesharwani, P., 2023a. Emerging application of magnetic nanoparticles for breast cancer therapy. Eur. Polym. J. 187, 111898 https://doi.org/10.1016/J.EURPOLYMJ.2023.111898.
Dongsar, T.T., Dongsar, T.S., Gupta, N., Almalki, W.H., Sahebkar, A., Kesharwani, P., 2023b. Emerging potential of 5-Fluorouracil-loaded chitosan nanoparticles in cancer therapy. J. Drug Deliv. Sci. Technol. 82, 104371 https://doi.org/10.1016/J.JDDST.2023.104371.
Fatima, M., Karwasra, R., Almalki, W.H., Sahebkar, A., Kesharwani, P., 2023. Galactose engineered nanocarriers: hopes and hypes in cancer therapy. Eur. Polym. J. 183, 111759 https://doi.org/10.1016/J.EURPOLYMJ.2022.111759.
Fereig, S.A., El-Zaafarany, G.M., Arafa, M.G., Abdel-Mottaleb, M.M.A., 2021a. Tacrolimus-loaded chitosan nanoparticles for enhanced skin deposition and management of plaque psoriasis. Carbohydr. Polym. 268, 118238 https://doi.org/10.1016/j.carbpol.2021.118238.
Fereig, S.A., El-Zaafarany, G.M., Arafa, M.G., Abdel-Mottaleb, M.M.A., 2021b. Self-assembled tacrolimus-loaded lecithin-chitosan hybrid nanoparticles for in vivo management of psoriasis. Int. J. Pharm. 608, 121114 https://doi.org/10.1016/J.IJPHARM.2021.121114.
Fiedler, H., Abad, E., de Boer, J., 2023. Analysis of persistent organic pollutants for the Stockholm Convention's global monitoring plan. Chemosphere 332. https://doi.org/10.1016/J.CHEMOSPHERE.2023.138843.
Ganesan, K., Wang, Y., Gao, F., Liu, Q., Zhang, C., Li, P., Zhang, J., Chen, J., 2021. Targeting engineered nanoparticles for breast cancer therapy. Pharmaceutics 13. https://doi.org/10.3390/PHARMACEUTICS13111829.
Gavas, S., Quazi, S., Karpiński, T.M., 2021. Nanoparticles for cancer therapy: current progress and challenges. Nanoscale Res. Lett. 16 https://doi.org/10.1186/S11671-021-03628-6.
Ghate, V.M., Kodoth, A.K., Shah, A., Vishalakshi, B., Lewis, S.A., 2019. Colloidal nanostructured lipid carriers of pentoxifylline produced by microwave irradiation ameliorates imiquimod-induced psoriasis in mice. Colloids Surf., B 181, 389–399. https://doi.org/10.1016/j.colsurfb.2019.05.074.
Gupta, P., Sheikh, A., Kesharwani, P., Abourehab, M.A.S., Abourehab, M.A.S., 2022. Amelioration of full-ThicknessWound using hesperidin loaded dendrimer-based hydrogel bandages. Biosensors 12. https://doi.org/10.3390/bios12070462.
Gyanewali, S., Kesharwani, P., Sheikh, A., Ahmad, F.J., Trivedi, R., Talegaonkar, S., 2021. Formulation development and in vitro–in vivo assessment of protransfersomal gel of anti-resorptive drug in osteoporosis treatment. Int. J. Pharm. 608, 121060 https://doi.org/10.1016/J.IJPHARM.2021.121060.
Hägerström, H., Edsman, K., 2003. Limitations of the rheological mucoadhesion method: the effect of the choice of conditions and the rheological synergism parameter. Eur. J. Pharmaceut. Sci. 18, 349–357. https://doi.org/10.1016/S0928-0987(03)00037-X.
Hamdi, M., Elmowafy, E., Abdel-Bar, H.M., ElKashlan, A.M., Al-Jamal, K.T., Awad, G.A. S., 2022. Hyaluronic acid-entecavir conjugates-core/lipid-shell nanohybrids for efficient macrophage uptake and hepatotropic prospects. Int. J. Biol. Macromol. 217, 731–747. https://doi.org/10.1016/j.ijbiomac.2022.07.067.
Het Cam, n.d.
Hirun, N., Dokmaisrijan, S., Tantishaiyakul, V., 2012. Experimental FTIR and theoretical studies of gallic acid-acetonitrile clusters. Spectrochim. Acta Part A Mol. Biomol. Spectrosc. 86, 93–100. https://doi.org/10.1016/j.saa.2011.10.009.
Imam, S.S., Ahad, A., Aqil, M., Akhtar, M., Sultana, Y., Ali, A., 2017. Formulation by design based risperidone nano soft lipid vesicle as a new strategy for enhanced transdermal drug delivery: in-vitro characterization, and in-vivo appraisal. Mater. Sci. Eng. C 75, 1198–1205. https://doi.org/10.1016/J.MSEC.2017.02.149.
Imam, S.S., Aqil, M., Akhtar, M., Sultana, Y., Ali, A., 2014. Formulation by Design-Based Proniosome for Accentuated Transdermal Delivery of Risperidone: in Vitro Characterization and in Vivo Pharmacokinetic Study. https://doi.org/10.3109/10717544.2013.870260 22.
Islam, F., Islam, M.M., Khan Meem, A.F., Nafady, M.H., Islam, M.R., Akter, A., Mitra, S., Alhumaydhi, F.A., Emran, T. Bin, Khusro, A., Simal-Gandara, J., Eftekhari, A., Karimi, F., Baghayeri, M., 2022. Multifaceted role of polyphenols in the treatment and management of neurodegenerative diseases. Chemosphere 307, 136020. https://doi.org/10.1016/J.CHEMOSPHERE.2022.136020.
Jagdale, S., Narwade, M., Sheikh, A., Md, S., Salve, R., Gajbhiye, V., Kesharwani, P., Gajbhiye, K.R., 2023. GLUT1 transporter-facilitated solid lipid nanoparticles loaded with anti-cancer therapeutics for ovarian cancer targeting. Int. J. Pharm. 637 https://doi.org/10.1016/J.IJPHARM.2023.122894.
Jahangir, M.A., Khan, R., Syed, Imam, S., Asadullah Jahangir, M., Sarim, S., 2017. Formulation of Sitagliptin-Loaded Oral Polymeric Nano Scaffold: Process Parameters Evaluation and Enhanced Anti-diabetic Performance. https://doi.org/10.1080/21691401.2017.1411933 46.
Kang, N.W., Kim, M.H., Sohn, S.Y., Kim, K.T., Park, J.H., Lee, S.Y., Lee, J.Y., Kim, D.D., 2018. Curcumin-loaded lipid-hybridized cellulose nanofiber film ameliorates imiquimod-induced psoriasis-like dermatitis in mice. Biomaterials 182, 245–258. https://doi.org/10.1016/j.biomaterials.2018.08.030.
Kapoor, H., Aqil, M., Imam, S.S., Sultana, Y., Ali, A., 2019. Formulation of amlodipine nano lipid carrier: formulation design, physicochemical and transdermal absorption investigation. J. Drug Deliv. Sci. Technol. 49, 209–218. https://doi.org/10.1016/J.JDDST.2018.11.004.
Karimi-Maleh, H., Darabi, R., Karimi, F., Karaman, C., Shahidi, S.A., Zare, N., Baghayeri, M., Fu, L., Rostamnia, S., Rouhi, J., Rajendran, S., 2023. State-of-art advances on removal, degradation and electrochemical monitoring of 4-aminophenol pollutants in real samples: a review. Environ. Res. 222, 115338 https://doi.org/10.1016/J.ENVRES.2023.115338.
Kesharwani, P., Jain, K., Jain, N.K., 2014. Dendrimer as nanocarrier for drug delivery. Prog. Polym. Sci. 39, 268–307. https://doi.org/10.1016/j.progpolymsci.2013.07.005.
Kesharwani, P., Sheikh, A., Abourehab, M.A.S., Salve, R., Gajbhiye, V., 2023. A combinatorial delivery of survivin targeted siRNA using cancer selective nanoparticles for triple negative breast cancer therapy. J. Drug Deliv. Sci. Technol. 80, 104164 https://doi.org/10.1016/J.JDDST.2023.104164.
Kongala, S.I., Mamidala, P., 2023. Harpin-loaded chitosan nanoparticles induced defense responses in tobacco. Carbohydr. Polym. Technol. Appl. 5, 100293 https://doi.org/10.1016/j.carpta.2023.100293.
Liu, Z., Parveen, N., Rehman, U., Aziz, A., Sheikh, A., Abourehab, M.A.S., Guo, W., Huang, J., Wang, Z., Kesharwani, P., 2023. Unravelling the enigma of siRNA and aptamer mediated therapies against pancreatic cancer. Mol. Cancer 2023 221 22, 1–22. https://doi.org/10.1186/S12943-022-01696-5.
Lu, J., Chen, Yi, Ding, M., Fan, X., Hu, J., Chen, Yihua, Li, J., Li, Z., Liu, W., 2022. A 4arm-PEG macromolecule crosslinked chitosan hydrogels as antibacterial wound dressing. Carbohydr. Polym. 277 https://doi.org/10.1016/J.CARBPOL.2021.118871.
Lu, J., Fan, X., Hu, J., Li, J., Rong, J., Wang, W., Chen, Ying, Liu, W., Chen, J., Chen, Yi, 2023. Construction and function of robust and moist bilayer chitosan-based hydrogel wound dressing. Mater. Des. 226, 111604 https://doi.org/10.1016/j.matdes.2023.111604.
Moolakkadath, T., Aqil, M., Ahad, A., Imam, S.S., Iqbal, B., Sultana, Y., Mujeeb, M., Iqbal, Z., 2018. Development of Transethosomes Formulation for Dermal Fisetin Delivery: Box–Behnken Design, Optimization, in Vitro Skin Penetration, Vesicles–Skin Interaction and Dermatokinetic Studies. https://doi.org/10.1080/21691401.2018.1469025 46.
Panonnummal, R., Jayakumar, R., Sabitha, M., 2017. Comparative anti-psoriatic efficacy studies of clobetasol loaded chitin nanogel and marketed cream. Eur. J. Pharmaceut. Sci. 96, 193–206. https://doi.org/10.1016/J.EJPS.2016.09.007.
Parmar, K.M., Itankar, P.R., Joshi, A., Prasad, S.K., 2017. Anti-psoriatic potential of Solanum xanthocarpum stem in Imiquimod-induced psoriatic mice model. J. Ethnopharmacol. 198, 158–166. https://doi.org/10.1016/J.JEP.2016.12.046.
Parveen, N., Abourehab, M.A.S., Thanikachalam, P.V., Khar, R.K., Kesharwani, P., 2023a. Nanocrystals as an emerging nanocarrier for the management of dermatological diseases. Colloids Surf., B 225, 113231. https://doi.org/10.1016/J.COLSURFB.2023.113231.
Parveen, N., Sheikh, A., Abourehab, M.A.S., Karwasra, R., Singh, S., Kesharwani, P., 2023b. Self-nanoemulsifying drug delivery system for pancreatic cancer. Eur. Polym. J. 190, 111993 https://doi.org/10.1016/J.EURPOLYMJ.2023.111993.
Pinto, M.F., Moura, C.C., Nunes, C., Segundo, M.A., Costa Lima, S.A., Reis, S., 2014. A new topical formulation for psoriasis: development of methotrexate-loaded nanostructured lipid carriers. Int. J. Pharm. 477, 519–526. https://doi.org/10.1016/j.ijpharm.2014.10.067.
Plaque Psoriasis: Global Drug Forecast and Market Analysis to 2030 - Market Research Reports & Consulting | GlobalData UK Ltd. [WWW Document], n.d.
Pradhan, M., Yadav, K., Singh, D., Singh, M.R., 2021. Topical delivery of fluocinolone acetonide integrated NLCs and salicylic acid enriched gel: a potential and synergistic approach in the management of psoriasis. J. Drug Deliv. Sci. Technol. 61, 102282 https://doi.org/10.1016/j.jddst.2020.102282.
Pramual, S., Lirdprapamongkol, K., Svasti, J., Bergkvist, M., Jouan-Hureaux, V., Arnoux, P., Frochot, C., Barberi-Heyob, M., Niamsiri, N., 2017. Polymer-lipid-PEG hybrid nanoparticles as photosensitizer carrier for photodynamic therapy. J. Photochem. Photobiol. B Biol. 173, 12–22. https://doi.org/10.1016/j.jphotobiol.2017.05.028.
Prasad, P.S., Imam, S.S., Aqil, M., Sultana, Y., Ali, A., 2014. QbD-based Carbopol Transgel Formulation: Characterization, Pharmacokinetic Assessment and Therapeutic Efficacy in Diabetes. https://doi.org/10.3109/10717544.2014.93653623.
Psoriasis Treatments: How to Get Rid of Psoriasis [WWW Document], n.d.
Pukale, S.S., Sharma, S., Dalela, M., Singh, A. kumar, Mohanty, S., Mittal, A., Chitkara, D., 2020. Multi-component clobetasol-loaded monolithic lipid-polymer hybrid nanoparticles ameliorate imiquimod-induced psoriasis-like skin inflammation in Swiss albino mice. Acta Biomater. 115, 393–409. https://doi.org/10.1016/j.actbio.2020.08.020.
Qadir, A., Aqil, M., Ali, A., Warsi, M.H., Mujeeb, M., Ahmad, F.J., Ahmad, S., Beg, S., 2020. Nanostructured lipidic carriers for dual drug delivery in the management of psoriasis: systematic optimization, dermatokinetic and preclinical evaluation. J. Drug Deliv. Sci. Technol. https://doi.org/10.1016/j.jddst.2020.101775.
Rachakonda, T.D., Schupp, C.W., Armstrong, A.W., 2014. Psoriasis prevalence among adults in the United States. J. Am. Acad. Dermatol. 70, 512–516. https://doi.org/10.1016/J.JAAD.2013.11.013.
Rahman, M., Alam, K., Ahmad, M.Z., Gupta, G., Afzal, M., Akhter, S., Kazmi, I., Jyoti, Ahmad, F.J., Anwar, F., 2012. Classical to current approach for treatment of

psoriasis: a review. Endocr. Metab. Immune Disord. - Drug Targets 12, 287–302. https://doi.org/10.2174/1871530312802002901.

Renzi, D.F., de Almeida Campos, L., Miranda, E.H., Mainardes, R.M., Abraham, W.-R., Grigoletto, D.F., Khalil, N.M., 2021. Nanoparticles as a tool for broadening antifungal activities. Curr. Med. Chem. 28, 1841–1873. https://doi.org/10.2174/0929867327666200330143338.

Sagdicoglu Celep, A.G., Demirkaya, A., Solak, E.K., 2022. Antioxidant and anticancer activities of gallic acid loaded sodium alginate microspheres on colon cancer. Curr. Appl. Phys. 40, 30–42. https://doi.org/10.1016/j.cap.2020.06.002.

Sharma, A., Upadhyay, D.K., Sarma, G.S., Kaur, N., Gupta, G. Das, Narang, R.K., Rai, V. K., 2020. Journal of Drug Delivery Science and Technology Squalene integrated NLC based gel of tamoxifen citrate for efficient treatment of psoriasis : a preclinical investigation. J. Drug Deliv. Sci. Technol. 56, 101568 https://doi.org/10.1016/j.jddst.2020.101568.

Sharma, V., Yusuf, M., Pathak, K., 2014. Nanovesicles for transdermal delivery of felodipine: development, characterization, and pharmacokinetics. Int. J. Pharm. Investig. 4, 119. https://doi.org/10.4103/2230-973x.138342.

Sheikh, A., Md, S., Alhakamy, N.A., Kesharwani, P., 2022. Recent development of aptamer conjugated chitosan nanoparticles as cancer therapeutics. Int. J. Pharm. 620, 121751 https://doi.org/10.1016/J.IJPHARM.2022.121751.

Siepmann, J., Peppas, N.A., 2012. Modeling of drug release from delivery systems based on hydroxypropyl methylcellulose (HPMC). Adv. Drug Deliv. Rev. 64, 163–174. https://doi.org/10.1016/J.ADDR.2012.09.028.

Singh, A., Ahmad, I., Akhter, S., Jain, G.K., Iqbal, Z., Talegaonkar, S., Ahmad, F.J., 2013. Nanocarrier based formulation of Thymoquinone improves oral delivery: stability assessment, in vitro and in vivo studies. Colloids Surf., B 102, 822–832. https://doi.org/10.1016/J.COLSURFB.2012.08.038.

Sun, J., Zhao, Y., Hu, J., 2013. Curcumin inhibits imiquimod-induced psoriasis-like inflammation by inhibiting IL-1beta and IL-6 production in mice. PLoS One 8, e67078. https://doi.org/10.1371/JOURNAL.PONE.0067078.

Sun, S.-J., Deng, P., Peng, C.-E., Ji, H.-Y., Mao, L.-F., Peng, L.-Z., Bae, K.H., Sun, S.-J., Deng, Peng, Peng, C.-E., Ji, H.-Y., Mao, L.-F., Peng, Li-Zeng, 2022. Extraction, structure and immunoregulatory activity of low molecular weight polysaccharide from dendrobium officinale. Polym 2022, 2899. https://doi.org/10.3390/POLYM14142899, 14, Page 2899 14.

Tambe, V.S., Nautiyal, A., Wairkar, S., 2021. Topical lipid nanocarriers for management of psoriasis-an overview. J. Drug Deliv. Sci. Technol. 64, 102671 https://doi.org/10.1016/j.jddst.2021.102671.

Xi, L., Lin, Z., Qiu, F., Chen, S., Li, P., Chen, X., Wang, Z., Zheng, Y., 2022. Enhanced uptake and anti-maturation effect of celastrol-loaded mannosylated liposomes on dendritic cells for psoriasis treatment. Acta Pharm. Sin. B 12, 339–352. https://doi.org/10.1016/j.apsb.2021.07.019.

Zeng, L., Gowda, B.H.J., Ahmed, M.G., Abourehab, M.A.S., Chen, Z.S., Zhang, C., Li, J., Kesharwani, P., 2023. Advancements in nanoparticle-based treatment approaches for skin cancer therapy. Mol. Cancer 2023 221 22 1–50. https://doi.org/10.1186/S12943-022-01708-4.

Zhang, J., Li, X., Wei, J., Chen, H., Lu, Y., Li, L., Han, L., Lu, C., 2018. Gallic acid inhibits the expression of keratin 16 and keratin 17 through Nrf2 in psoriasis-like skin disease. Int. Immunopharm. 65, 84–95. https://doi.org/10.1016/j.intimp.2018.09.048.

Zhao, G., Shi, L., Yang, G., Zhuang, X., Cheng, B., 2023. 3D fibrous aerogels from 1D polymer nanofibers for energy and environmental applications. J. Mater. Chem. 11, 512–547. https://doi.org/10.1039/D2TA05984C.